Dielectric Liquid Ionization Chambers for Detecting Fast Neutrons

by

Erin M. Boyd

B.S. Physics, Spelman College (2004)

Submitted to the Department of Nuclear Science & Engineering
in partial fulfillment of the requirements for the degree of

Master of Science

at the

MASSACHUSETTS INSTITUTE OF TECHNOLOGY
[February 2008]
September 2007

Author.....
Department of Nuclear Science & Engineering
September 10, 2007

Certified by.....
Richard Lanza
Senior Research Scientist
Department of Nuclear Science & Engineering
Thesis Supervisor

Certified by.....
Dwight Williams
MLK Visiting Professor
Department of Nuclear Science & Engineering
Thesis Reader

Accepted by.....
Jeffery Coderre
Chairman, Departmental Committee on Graduate Students
Department of Nuclear Science & Engineering

Dielectric Liquid Ionization Chambers for Detecting Fast Neutrons

by

Erin Boyd

Submitted to the Department of Nuclear Science & Engineering

on September 10, 2007, in partial fulfillment of the requirements for the degree of

Master of Science in Nuclear Science & Engineering

Abstract

Three ionization chambers with different geometries have been constructed and filled with dielectric liquids for detection of fast neutrons. The three dielectric liquids studied were Tetramethylsilane (TMS), Tetramethylpentane (TMP), and Isooctane, which each have intrinsic properties that make them attractive for fast neutron detection. Their electronic properties are similar to those of condensed noble gases, but they don't require cryogenic temperatures to maintain liquid phase. However, like condensed noble gases, they do require a high level of purity.

A stainless steel purification system was constructed to purify the liquids and the purity was monitored by an ionization chamber with a ^{241}Am source inside. The three liquid detectors were exposed to 250keV x-rays from an orthovoltage x-ray tube and neutrons (1.4-12MeV) from a 1-Ci ^{239}Pu-Be source.

Experimental data show that an ionization chamber filled with dielectric liquid is capable of detecting fast neutrons in pulse mode. While chamber 1, chamber 2, and chamber 3 (filled with TMS) did not respond to the Pu-Be source, chamber 3 (filled with TMP and Isooctane) successfully detected the presence of neutrons. Data also show that the chambers could not detect gamma rays from 1μCi Co-60 and Cs-137 check sources. In addition, the chambers could detect 250 keV x-rays in current mode, but not pulse mode. These results present positive implications for the gamma-blindness of the dielectric liquids studied.

Thesis Supervisor: Dr. Richard Lanza
Title: Senior Research Scientist

Acknowledgements

I would like to thank Dr. Richard Lanza for his supervision, financial and intellectual support, and patience throughout my time at MIT. He has been an enormous source of information and I have learned very much.

Many thanks go to Dr. Gordon Kohse. I honestly don't know if I could have completed this work without his unlimited support and assistance. Gordon listened to each of my ideas and helped me implement them. Words cannot express how much I appreciate his guidance.

I thank Dr. Dwight Williams for his moral support and careful reading of this thesis. I can't thank Dwight enough for flying to Boston on a Sunday morning, just to sign my thesis, and immediately flying back to Washington D.C.

Additional thanks go to MITR RPO and MIT Reactor staff for allowing me to use their laboratory space to run my experiments and to the Nuclear Science and Engineering Department for allowing me to study at MIT.

Finally, I thank the deans and staff in the Graduate Students Office. They have supported me since I arrived at MIT and I am extremely appreciative.

Contents

List of Figures

List of Tables

Chapter 1

Introduction

Fast neutrons have proven to be extremely useful in various facets of research and industry. Two necessary processes used in neutron applications are neutron production and detection. While fast neutron production has been successfully accomplished by different methods, neutron detection has not been easy to master. The major challenges encountered with neutron detection are high energy photon background noise, neutron neutrality, recombination, multiple events, and spatial resolution to name a few. These factors cause the efficiencies of modern-day fast neutron detectors to be extremely low.

The type of neutron detector that should be used for a given application depends on factors such as the initial neutron energy and the goals of the specific neutron application. Depending on the neutron application, the ability to count neutrons in the vicinity of the detector may be sufficient. However, if the detector is required to measure the initial energy of the neutrons, the detector design becomes more complex. Regardless of what function the detector performs, its effectiveness is highly dependent upon its efficiency. Thus, there is a clear need for higher efficiency neutron detectors.

This thesis examines the design and operation of a dielectric liquid ionization chamber which is used for detecting neutrons with a higher efficiency than existing neutron detectors.

1.1 Neutron Detection

Neutron detection is performed through indirect methods because, like photons, neutrons are uncharged particles. Due to the charge neutrality of neutrons, they do not interact with the electrons of an atom in matter. Rather, they interact with the nucleus of that atom. In other words, they do not respond to Coulomb force. Charged particles,

such as protons, alphas, betas, etc. are the result of such nuclear interactions. The electrical signals generated from these charged particles are processed for detection. Direct detection of the charged particles, in turn, indirectly detects the neutrons.

The technique used for neutron detection is dependent upon the neutron energy because the cross section for neutron interactions in materials is a function of neutron energy. For neutrons that have energies below 0.5eV, neutron-induced nuclear reactions are the most common interaction for detection purposes. As the neutron energy increases, scattering becomes a more dominant interaction. Elastic scattering is the most probable neutron interaction at neutron energies above 0.5eV, but when the neutron energy is sufficiently high, inelastic scattering with nuclei may occur.

1.1.1 Slow Neutron Detection

Slow neutrons are defined as neutrons with kinetic energy less than 0.5eV. At these energies, the significant neutron interactions are neutron-induced nuclear reactions and neutron elastic scattering with target nuclei. The most common means of detecting slow neutrons are based on neutron-induced nuclear reactions because very little energy can be transferred to the target nuclei during an elastic collision caused by a slow neutron.

Neutron-Induced Nuclear Reactions

Neutron-induced nuclear reactions that are employed for detection create secondary radiation that has enough energy to be directly detected. In order for these particular reactions to occur, the Q-values for these reactions must be positive. The Q-value is the energy equivalent of the difference in atomic masses between the reactants and products, all in their nuclear ground states. Q-value is calculated using equation 1.1.

$$Q \equiv [(M_1 + M_2) - (M_{1'} + M_{2'})]c^2 \qquad \text{Eq. 1.1}$$

where M_1 is the incoming particle, M_2 is the target nucleus, $M_{1'}$ is the outgoing particle and $M_{2'}$ is the recoil nucleus.

The Q-values of the reactions, rather than the energy of the incoming slow neutron, determine the kinetic energy of the reaction products. This is because the Q-value is typically sufficiently greater than that of the incoming neutron.

The most probable reaction that occurs from neutron-induced nuclear reactions is radiative capture (n, γ). This reaction is not often used to detect neutrons because, like neutrons, it is also difficult to detect gamma rays due to their neutrality. More common reactions used for neutron detection are (n, α), (n, p), and (n, fission fragment). Each of these common neutron detection reactions results in heavy charged particles. The three most popular reactions and their Q-values can be found in table 1.1.

Table 1.1 Neutron-induced nuclear reactions for slow neutron detection

Reaction Name	Reaction	Q-value
$^{10}B(n,\alpha)$	$^{10}B_5 + {}^1n_0 \rightarrow {}^7Li_3 + {}^4\alpha_2$ $^{10}B_5 + {}^1n_0 \rightarrow {}^7Li_3^* + {}^4\alpha_2$	2.792 MeV (ground state) 2.310 MeV (excited state)
$^6Li(n,\alpha)$	$^6Li_3 + {}^1n_0 \rightarrow {}^3H_1 + {}^4\alpha_2$	4.78 MeV
$^3He(n,p)$	$^3He_2 + {}^1n_0 \rightarrow {}^3H_1 + {}^1p_1$	.764 MeV

*excited state

Neutron-induced fission reactions, although not listed in the table above, are also utilized for slow neutron detection. Common interaction materials for fission reactions are ^{233}U, ^{235}U and ^{239}Pu. The Q-value for these reactions is roughly 200 MeV. Due to the high Q-value, these reactions can produce larger output pulses than the reactions previously mentioned. Nevertheless, detectors that exploit the fission reaction have disadvantages such as low efficiency and reduced speed.

Slow Neutron Elastic Scattering

As previously stated, elastic collisions are very probable neutron interactions. Depending on its initial energy, the neutron may be stopped or moderated as a result of the collision with a target nucleus. If the incoming slow neutron happens to have enough energy to produce a recoil nucleus, the energy transfer would still be too low to generate a measurable signal from the recoil nuclei. Thus, elastic scattering is not very useful in

detecting slow neutrons. However, neutrons with energies in the keV range are much more successful at producing recoil nuclei with enough energy to create a discernible signal; thus, the method of using elastic scattering for detection is much more applicable for detecting fast neutrons.

1.1.2 Fast Neutron Detection

There are four methods used to detect fast neutrons – moderation, neutron-induced reactions, fast neutron elastic scattering and fast neutron inelastic scattering. The decision of which method to exploit is based on various motivations. One such motivation is whether or not the kinetic energy of the incoming neutron needs to be measurable. Fast neutron detection based on moderation, inelastic scattering, and neutron-induced reactions, depending on the neutron's energy with respect to the Q-value, cannot extract energy information. However, detection based on elastic scattering retains this capability. Detectors that simply record the presence of fast neutrons without measuring incoming energy can be based on any of the four methods.

Moderation

Technically, any of the reactions used to detect slow neutrons can be employed to detect fast neutrons, but the efficiency of such detectors would be extremely low. This low efficiency is a consequence of the fact that the cross-section of the neutron-induced reactions decreases as neutron energy increases. This feature can be seen in figure 1.1.

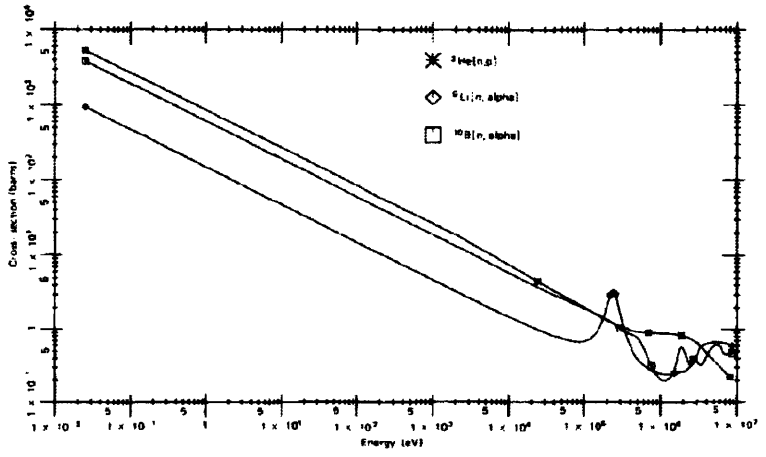

Figure 1.1 Cross Section Energy Dependence for Popular Neutron-Induced Reactions [1].

This complication can be improved by incorporating moderation. Moderators are materials that incoming fast neutrons interact with before reaching the detector. As a result of the neutron-moderator interaction, some or all of the neutron's kinetic energy is lost in the moderator. Thus, by the time the neutron reaches the detector, it would have experienced enough collisions within the moderator such that its energy is low enough to be detected with a greater efficiency.

Although this technique works, there are a few disadvantages. Firstly, the efficiency of the detector is lowered by the possibility of the neutrons being stopped in the moderator and never reaching the detector. At low neutron energies, the neutron absorption cross-section dominates over elastic collisions. Secondly, moderation eliminates all initial energy information. Lastly, moderation slows down the detection process; thus, this method lacks the fast detection required of many neutron detection applications.

Neutron-Induced Reactions

This method of detecting fast neutrons has a much lower efficiency than moderation because the cross-section for these neutron-induced reactions is much lower at high neutron energies than at thermal energies. However, this method resolves each of the disadvantages that exist when utilizing moderation.

Two neutron-induced reactions that are exploited when detecting fast neutrons are $^{3}He(n,p)$ and $^{6}Li(n,\alpha)$. The initial neutron energy can be extracted by subtracting the Q-value of the reaction from the kinetic energy of the reaction products. Also, the lack of moderator eliminates the travel time through the moderator as well as the possibility of the neutron being absorbed in the moderator and never being detected.

Elastic Scattering

Neutron elastic scattering is the transfer of all or a portion of the kinetic energy from incoming neutron to the scattering nucleus. This interaction results in a recoil nucleus and usually a scattered neutron. Unlike the case of neutron-induced reactions, the Q-value of an elastic scattering reaction is zero because the energy before and after

the reaction is the same by definition. Thus, the kinetic energy of the incident neutron is equal to the sum kinetic energy of the recoil nucleus and the scattered neutron.

This method is most commonly exploited when detecting fast neutrons because the elastic scattering cross-section is highest for fast neutrons and initial energy information can be extracted. However, there are characteristics of this method that negatively affect efficiency such as multiple scattering events, which are discussed in section 1.4.2.

Inelastic Scattering

Neutron inelastic scattering is unlike elastic scattering because the target nucleus is no longer kept in the ground state after the collision. The incoming neutron transfers enough energy to the target nucleus to cause it to leave the ground state and become excited. This excited energy is equal to the negative Q-value. Thus, neutron inelastic scattering is an endothermic process. In other words, in order for this reaction to occur, the neutron energy must exceed the characteristic threshold for the target element. Eventually, the excited nucleus will de-excite, usually producing characteristic gamma rays in the process. The resulting gamma rays from the (n, n', γ) reaction are detected. Gamma rays are necessary for this method of neutron detection, but they could be considered a complication when another method, such as proton recoil, is utilized to detect neutrons.

1.2 Fast Neutron Detectors

This thesis concentrates more specifically on the detection of fast neutrons; thus, discussion of detectors used to detect neutrons in the thermal to slow energy ranges will not be incorporated in the following sections. Also, since the most common technique employed to detect fast neutron is elastic scattering, the detectors discussed in this section are based on that method.

1.2.1 Scintillation Detectors

Scintillators that detect fast neutrons are usually hydrogenous. Incoming fast neutrons that encounter the scintillator interact with the hydrogen nuclei and produce

recoil protons. These recoil protons then collide with atomic electrons existing within the scintillation material causing them to become excited. As de-excitation occurs, light is emitted. Although counting neutrons can be done by counting the number of fluoresces that occur, the energy of the incoming neutron cannot be measured. This is because the emitted light is not an indicator of the energy of the incoming neutron; rather it contains information about the energy of the recoil proton.

The three types of scintillators discussed in this section are organic crystals, organic liquids, and plastics. Each of these scintillators is hydrogenous and relies on proton recoil.

Organic Crystal Scintillators

Crystal scintillators are organic molecules that have a structure that incorporates one or more benzene-like rings. The formula for the organic chemical compound, Benzene, is C_6H_6. When pure, these molecules form crystals. Scintillation occurs when the ionizing radiation excites the outer shell electrons in the benzene ring and those electrons de-excite and recombine with the holes.

The scintillation efficiency, η, is defined as:

$$\eta \equiv \frac{E_{SL}}{E} = \frac{h\upsilon_e}{\omega} Tq \qquad \text{Equation 1.2}$$

where $h\upsilon_e$ is the average energy of the emitted photon, E_{SL} is the energy of the scintillation light, E is the energy deposited, T is the energy transfer efficiency from excited ion to luminescence center, q is the quantum efficiency of luminescence center, and ω is the energy required to create one electron-hole pair. Based on equation 1.2, the efficiency of one of the best known organic scintillators, anthracene, is roughly 4 percent [2]. Thus, the absolute scintillation efficiency is small. Most of the deposited energy is lost by phonons, which are vibrations that occur in the atomic lattice of the crystal.

Plastic Scintillators

Various techniques can be applied to manipulate the structure and/or phase of the scintillation material. An example of this is the formation of an organic plastic scintillator. This scintillator is created by dissolving the organic crystal in a transparent polymer solution that becomes solid at ambient temperature. The plastic is typically highly machinable. The use of organic plastic scintillators to detect fast neutrons is widespread for reasons such as their modest cost, fast response time (a few nanoseconds), and good transparency to their own radiation. In conjunction with these advantages, the major disadvantage of detecting fast neutrons with organic scintillation material still exists. Unfortunately, scintillators have high gamma ray sensitivity and neutron-gamma discrimination is a challenging, yet necessary prerequisite to identifying fast neutrons.

Table 1.2 is a list of some well known organic plastic scintillators and their important properties.

Table 1.2 List of well known organic plastic scintillators [7].

Commercial Name	Light Output (% anthracene)	Wavelength of Maximum Emission (nm)	H/C Ratio	Decay Constant (ns)	Typical Light Attenuation Length (cm)	Principal Applications
NE-102A	65	423	1.103	2.4	250	General applications
NE-104	68	408	1.107	1.8	160	Fast timing
Pilot U	67	391	1.107	1.4	n/a	Ultra fast timing
Pilot F	64	425	1.104	2.1	380	Best overall general properties

The intrinsic efficiency of organic plastic scintillators is defined as:

$$\varepsilon = \frac{N_H \sigma_H}{N_H \sigma_H + N_C \sigma_C + N_{Si} \sigma_{Si}} \cdot (1 - e^{-d(N_H \sigma_H + N_C \sigma_C + N_{Si} \sigma_{Si})}) \qquad \text{Equation 1.3}$$

where N is the nuclear number density of the target nuclei, σ is the scattering cross section, and d is the pathlength through the detector for incident neutrons (detector thickness).

Organic Liquid Scintillators

Organic crystals can also be liquefied by dissolving them in a transparent liquid. Depending on the purity and concentration of the liquid, properties similar to the organic crystal are preserved. Organic liquid scintillators can be used to detect gamma rays, beta particles, alpha particles, and neutrons. They are especially applicable when pulse shape discrimination is necessary because they have relatively high light-output, reasonably good efficiency for fast neutrons, fast decay time of the light output, and a slow component which depends on the energy loss density [14]. Pulse shape discrimination exploits the characteristics of neutron and gamma ray pulses in order to differentiate between the two. Various methods can be used to perform this task, some of which are discussed in section 1.4.4. Typically, liquid scintillators are low cost and useful when large detection volumes are required. Also, most organic liquid scintillators have good transparency to their own radiation.

While there are many benefits of using organic liquid scintillators to detect fast neutrons, the fact that scintillators are extremely sensitive to gamma rays is not advantageous. In other words, when employing organic liquid scintillators for fast neutron detection, neutron-gamma discrimination is required. The degree of discrimination liquid scintillators offer against gamma rays is inadequate when gamma-ray flux is large [16]. Also, when count rates are high, performance is limited by pulse pile-up because liquid scintillators produce relatively long pulses. Other difficulties in performing pulse shape discrimination are discussed in section 1.4.4.

Table 1.3 lists well known organic liquid scintillators and their important properties.

Table 1.3 List of well known organic liquid scintillators [7].

Commercial Name	Light Output (% anthracene)	Wavelength of Maximum Emission (nm)	H/C Ratio	Decay Constant (ns)	Principal Applications
NE-213	78	425	1.211	3.2	PSD, fast neutron/gamma discrimination
NE-224	80	424	1.331	2.5	High light output
NE-228	45	385	2.111	-	High H/C ratio

1.2.2 Gas Proportional Counters

Gas proportional counters are used as an alternative to scintillators. Typically, they are cylindrical tubes filled with hydrogen, methane, or another low Z gas such as helium. Generally, there is an anode wire running through the center of the cylinder and the detector wall serves as the cathode. High voltage is applied to one or both of the electrodes to create an electric field region. The electrons are attracted to the positive field region and the positively charged particles are attracted to the negatively charged (or grounded) electrode.

A major advantage of gas proportional counters is the multiplication feature. The electric field near the axial wire accelerates the approaching electrons to energies so high that their collisions with the gas molecules cause further ionization. This effect, called gas multiplication, increases the pulse size by factors of hundreds or thousands. As a result, proportional counter pulses are in the millivolt rather than microvolt range. Consequently, electronics used for external amplification may not be necessary.

On the other hand, there are significant disadvantages of gas proportional counters such as lower efficiency due to the gaseous detection medium. In fact, the efficiency for detecting neutrons in the MeV energy range with a gas proportional counter is typically less than 1 percent [1]. The low neutron interaction probability in the fill gas is considered disadvantageous for the most part, but there is one benefit – multiple scattering events normally do not influence the response function. Multiple scattering

events occur when the scattered neutrons interact in the detection medium. As a result of the low interaction probability, primary scattering is infrequent and secondary scattering is implausible.

Other challenges with detecting neutrons with a gas proportional counter are maintaining gas purity and gamma ray interactions with the walls of the proportional counter. Gas purity is extremely important when operating a gas proportional counter as even microscopic air leaks will cause the detector to fail. To maintain the gas purity it is necessary to routinely check for leaks and exercise extreme care when handling the detector. Gamma ray interactions are an issue when trying to detect neutrons with an organic scintillator because there is 2 to 3 times more light output from electrons produced by gamma ray interactions than from charged particles (i.e. recoil protons) produced from neutron interactions. This problem is amplified in gas proportional counters because not only do gamma rays interact with the fill gas, but they also interact with the walls of the counter. This wall interaction results in secondary electrons that may escape into the fill gas. Thus, the number of gamma ray pulses is presumably higher in a gas proportional counter than in an organic scintillator with the same elemental composition.

1.3 Fast Neutron Detector Applications

Various neutron detectors have been created and considered over the years because they are a necessary component of utilizing nuclear-based technologies. As neutron applications gain popularity in industry and research, the efficient detection of neutrons becomes a prerequisite to successful nuclear-based technology implementation. Although neutron detectors have many practical applications, this section discusses a few of the most prevalent.

1.3.1 Reactors

Nuclear reactors have many uses, but the most common is energy generation. Commercial reactors function by sustaining a chain of nuclear fission reactions. The fission reaction occurs when nuclear fuels breed neutrons and fission products when

triggered by free neutrons. For safety purposes, the vicinities of reactors are monitored by detectors. An efficient neutron detector is advantageous for promoting safe operating conditions.

1.3.2 Fast Neutron Resonance Radiography

Fast Neutron Resonance Radiography (NRR) is a nuclear technique that provides two-dimensional elemental information about materials. This procedure has application in security and material analysis. Currently, the method used to perform NRR encompasses a neutron source that produces fast neutrons and a hydrogenous scintillator that detects neutrons that are attenuated through an object. Once the neutrons are detected and the light is emitted from the scintillator, a CCD camera produces a radiographic image. A radiographic image is a two-dimensional map of the weighted sum of projected elemental contents [6]. By exploiting the resonance peaks in total attenuation cross sections of various elements, the penetrated element can be identified. When detecting explosives and drugs, the significant elements are nitrogen, hydrogen, oxygen and carbon.

While this detection method works in theory, in practice, achieving desired results is complicated for reasons such as low detection efficiency and gamma contamination.

1.4 Fast Neutron Detector Limitations

Performing efficient fast neutron detection is a challenging task. Neutron detectors have low performance capabilities for a variety of reasons. Some limitations are attributable to the intrinsic properties of neutrons and others are due to the specific characteristics of the detector. Most neutron detectors are designed to increase efficiency by addressing particular detection limitations, but after years of attempting to achieve higher efficiencies, there is still much room for improvement.

1.4.1 Recombination

As previously discussed, when detecting fast neutrons using elastic scattering methods, the incoming neutron ionizes the atoms of the target material. The charged particles that are the products of the scattering event are directly detected, which oper

ates as an indirect detection of the incoming neutron. The activity of the charged particles between the time of ionization and the time of detection is significant to the efficiency of the detector. If the positive ions and the negative ions (or free electrons) interact between ionization and detection, they may recombine and become neutralized. Once the ions are neutralized, a detector based on charge collection can no longer deliver a signal. This process of neutralization is called recombination. Recombination depends on the particle's ionization density and the external electric field. The more densely ionizing a particle is, the more susceptible it is to recombination. In contrast, the rate of recombination decreases with increasing external electric field [15]. Recombination lowers detection efficiency because neutrons that were present will not be detected due to neutralization of charges. In addition, smaller signals are often observed due to high ionization density.

1.4.2 Multiple Elastic Scattering Events

Typically, hydrogen nuclei are used as the target because 0 to 100 percent of the neutron energy can be transferred; thus, providing the best chance of a single scattering event. Taking the average, half of the initial neutron energy is transferred to the recoil proton and the other half exists as the energy of the scattered neutron. If the scattered neutron encounters another nucleus, a subsequent scattering event could occur. This multiple scattering generates an exaggerated neutron count. Decreasing the size of the detector can mitigate this problem because doing so increases the chances of the scattered neutron escaping the detector before colliding with another nucleus.

1.4.3 Spatial Resolution

Spatial resolution is the measure of how finely detail can be resolved in space; thus, it is an important consideration for imaging applications. Spatial resolution influences the efficiency of neutron detectors, specifically scintillators, because it limits the thickness of the detector (scintillator). According to equation 1.3, a thicker scintillator will optimize efficiency, but a thinner scintillator will optimize spatial resolution. In other words, the thicker a detector, the bigger the spatial resolution sacrifice. Spatial resolution deteriorates with increasing detector thickness because, as

denoted in equation 1.4, the full-width at half-maximum (FWHM) of the spatial resolution line-spread function (LSF) is roughly directly proportional to the thickness of the scintillator. The FWHM of the LSF is the spatial resolution. A large FWHM value represents poor spatial resolution.

$$FWHM = \frac{d}{L} \qquad \text{Equation 1.4}$$

d is the scintillator thickness and L is the distance between the scintillator and the neutron source.

1.4.4 Gamma Interactions

A reoccurring problem with detecting fast neutrons is distinguishing them from gamma rays. A neutron detector can usually be protected from charged particles by deflection of the latter in a magnetic field or by an absorber that only modestly attenuates the flux of incoming neutrons [3]. In contrast, since gamma rays have no charge, the magnetic field is ineffectual and absorbers are not effective because gamma rays are almost as penetrating as neutrons.

In organic scintillation detectors, energy that is deposited in the scintillator by protons and alpha particles is produced by neutrons and energy that is deposited by electrons is produced by gamma rays [3]. In theory, the pulse shapes from multiple neutron interactions should be broader than that of multiple gamma interactions because the speed at which gamma rays travel between successive interactions is higher than that at which neutrons travel. For example, neutrons with an energy of 1.0 MeV travel at a speed of 1.4 cm/ns, whereas gamma rays travel at 30cm/ns. Thus, light should be emitted at two different times and at different durations. The first light emission would be the gamma ray contribution and the second would be the neutron contribution. Figure 1.2 illustrates what a gamma ray and neutron pulses might look like.

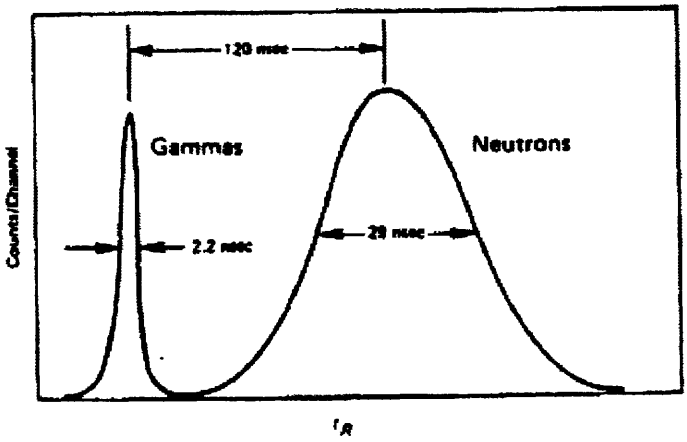

Figure 1.2 Calculated Response for a 100keV electron and 500keV neutron [5].

As previously stated, theoretically the detector is able to differentiate gamma ray pulses from neutron pulses, but in practice this is not the case. Due to variables such as the PMT response, scintillator response, and optical delays, the gamma ray pulses experience a broadening effect. Thus, the gamma ray and neutron pulses become indistinguishable. Another concern is that discerning fast neutrons under these conditions is even more difficult because as their energy increases, their response times and pulse heights become more comparable to that of some gamma rays.

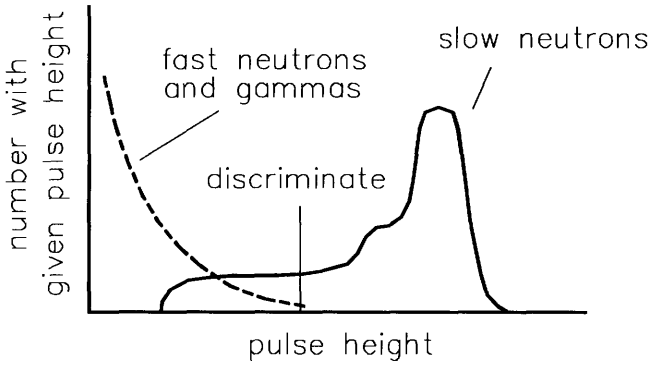

Figure 1.3 Example of a graph formulated from pulse height/shape analysis [8].

Various techniques such as pulse shape analysis, 10% to 90% risetime measurements, and time-of-flight have been used to discriminate neutron and gamma pulses. A graph formulated from pulse height analysis may look something like figure

1.3. Although successful in some situations, these techniques are imperfect and often inadequate.

Neutron-Gamma Discrimination Methods

Pulse shape analysis is the comparison of pulse height and/or pulse width, which was just discussed. The risetime measurement observes the output pulse from a charge integrating preamplifier and the tail (10% to 90%) of the pulse is known as the risetime. The risetimes of gamma rays are typically 10-20ns and 40-100ns for fast neutrons. The analysis is usually done by plotting risetime against pulse height as seen in figure 1.4.

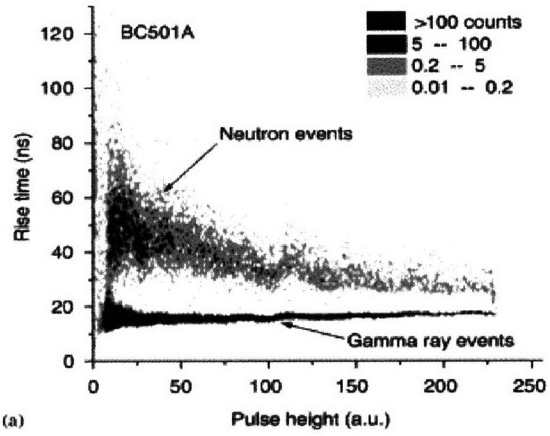

Figure 1.4 Risetime vs. pulse height plot at low-gain setting showing n/γ PSD from a BC501A scintillator [17].

Time-of-flight measurements use the difference in neutron/gamma ray travel speed to discriminate between the two particles. One method of performing a time-of-flight measurement is by exposing a neutron/gamma ray source to two low density scintillators separated by an air gap and comparing the amount of time it takes for the particles to traverse the air gap [16]. The results obtained in [16] show that when the air gap is 30 cm the travel time for gamma rays is 1 ns and 22ns for 1MeV neutrons.

1.5 Room Temperature Liquid Ionization Chamber for Fast Neutron Detection

Ionization chambers are by no means new to the scene of charged particle detection. In fact, they are considered to have the simplest construction of all charged particle detectors. Ionization chambers typically consist of two metal electrodes, a fill medium, and an enclosure. The fill medium is usually gas, but can also be solid or liquid. Voltage is applied between the electrodes; therefore, generating an electric field. Ionizing radiation (x-rays, neutrons, alpha particles, etc...), passing through the sensitive volume of the detector will interact with the molecules of the fill medium causing the neutral molecules to become excited or ionized. The ionization of the molecules results in the formation of a positive ion and free (negatively charged) electron, collectively called an ion pair. A minimum amount of energy must be transferred from the ionizing radiation to the neutral molecule in order for ionization to occur. This minimum energy, which is a function of the particular fill medium, is called the ionization energy of the molecule. However, the ionizing particles may lose energy inside the fill medium through mechanisms that do not lead to ion pairs. Hence, the energy lost by ionizing particles that create ion pairs is typically larger than the actual ionization energy of the molecule. The energy lost by the ionizing particles that create ion pairs, called the w-value, depends on the particular fill medium, the type of ionizing radiation, and its energy.

Once an ion pair is formed, the presence of the electric field causes the ions to move apart along the electric field lines toward the electrode of opposite polarity. This charge movement generates ionization current. When the ions reach their respective electrodes, they deposit or remove a small electric charge to or from the electrode. This rearrangement of charge can be measured and indicates detection of the incoming ionizing radiation.

1.5.1 Chamber Geometry

Depending on the application, certain ionization chamber geometries may be better suited than others. Many different geometric designs are compatible with

ionization chamber functionality because the chamber's operation requires very few elements and those elements can be easily altered without hindering chamber's function. The number of conceivable ionization chamber geometries is too many to identify here, but three of the more common geometries are discussed below.

Parallel Geometry

The most basic design for an ionization chamber is an enclosure with two metal parallel plates separated a distance apart and a detection medium between them. It is not always necessary to use two plates. When the enclosure is made of a conducting material, the wall of the enclosure can be used as an electrode.

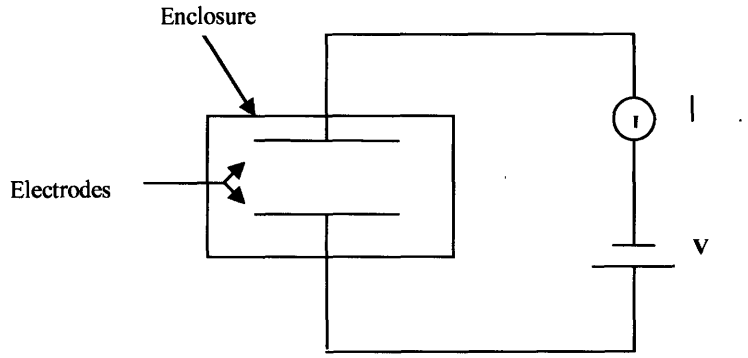

Figure 1.5 Basic parallel plate ionization chamber and electronic components.

Voltage is applied to one plate while the other is either at ground or a negative potential. The resulting electric field is uniform between the plates, which is an advantage the planar geometry has over cylindrical geometry. The electric field for planar geometry is given by

$$E = \frac{V}{d} \qquad \text{Equation 1.5}$$

where V is the voltage across the plates and d is the space between them. The electric field lines for planar geometry are illustrated in the field map below.

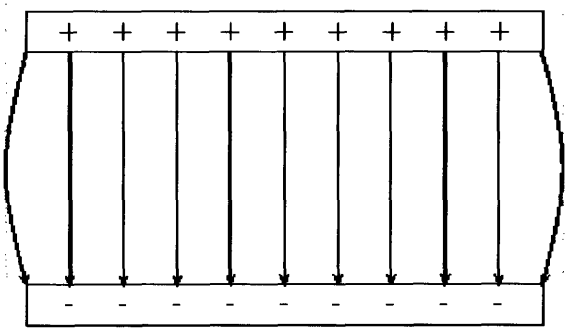

Figure 1.6 Electric field map for oppositely charge parallel plates

The electric field is uniform between the plates, except at the edges. When the ratio of plate length to plate separation gets too small (i.e. the plates are not long enough and/or the distance is too large) the field becomes non-uniform, particularly at the edges. This is called a fringe field.

Cylindrical Geometry

Another common ionization chamber construction is the cylindrical geometry. Cylindrical ionization chambers are constructed out of two concentric tubes, an outer cylinder and a central rod, or an outer cylinder and a central wire. In both cases, the outer cylindrical shell is normally operated at ground potential and the central conductor carries the applied voltage. The outer cylinder also functions as the enclosure; therefore, it must be sealed on both ends.

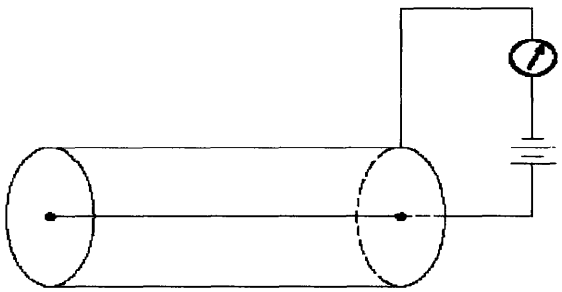

Figure 1.7 Basic cylindrical ionization chamber and electronic components.

The electric field generated using cylindrical geometry varies inversely with radius.

$$E = \frac{V}{r \ln(b/a)} \qquad \text{Equation 1.6}$$

where V is the voltage applied between the anode and cathode, a is the anode radius, and b is the cathode inner radius.

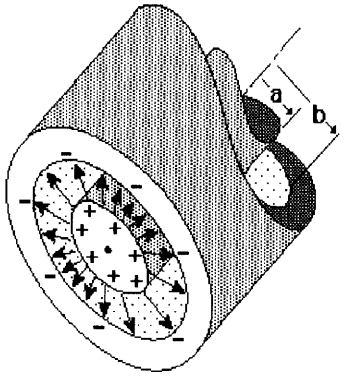

Figure 1.8 Illustration of field lines for oppositely charged cylindrical electrodes [8].

A feature of this geometry is that a much higher electric field can be achieved at the anode of the cylindrical chamber than can be reached using the planar geometry, assuming the same applied voltage. Thus, for applications that require high electric fields, cylindrical geometry may be more appropriate than planar. The radial dependence of the electric field; however, is a complication of the cylindrical geometry that the planar geometry lacks. Determining the field throughout a cylindrical chamber, as well as current-voltage characteristics is a complex problem. Analytical methods can be utilized to perform those calculations.

Spherical Geometry

Ionization chambers with spherical geometry consist of an inner sphere surrounded by a concentric outer shell. Similar to cylindrical ionization chambers, the outer shell can function as the enclosure. Generally, the outer shell is negatively charged or at ground, while the inner sphere is positively charged. With this charge arrangement, the electric field points radially outward from positive to negative (or ground).

$$E = \frac{V}{r^2[\frac{1}{a} - \frac{1}{b}]} \qquad \text{Equation 1.7}$$

where V is the voltage applied between the anode and cathode, a is the radius of the inner sphere, and b is the radius of the outer shell.

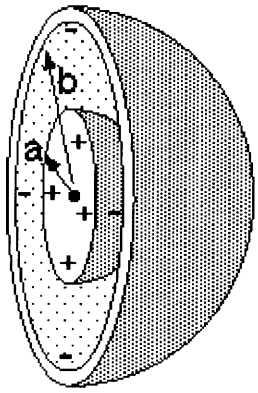

Figure 1.9 Cross-section of oppositely charged spherical conductors [13].

An advantage of utilizing this geometry for radiation detection is that a nearly uniform response to radiation from every direction can be achieved. This uniform omni-directional response is especially useful when detecting isotropic radiation such as neutrons. However, like cylindrical ionization chambers, spherical ionization chambers have a non-linear electric field. The field varies inversely with radius squared; thus, finding the electric field throughout the chamber is complicated and typically requires analytical methods.

1.5.2 Modes of Operation

Ionization chambers can be run in current mode or pulse mode. The operational mode exploited is based on the application. For example, when the event rate is very high, current mode operation is conventional. However, when the energy of incoming radiation needs to be determined, pulse mode operation is necessary. Additionally, detectors that are designed to count individual particles of radiation are operated in pulse mode.

Pulse Mode

Pulse mode detects individual ionizing particles. The output of a detector operated in pulse mode exhibits single pulses that are each representative of the interaction of a single particle of incoming radiation. In other words, the occurrence of a pulse signifies an interaction event caused by a single incoming particle of radiation. The amount of charge produced by the interaction is indicated by the pulse amplitude.

This mode of operation is essential for determining the energy of the individual incoming radiation particles. However, at high count (event) rates, detection in pulse mode is unrealistic because pulses begin to overlap. The circuit for pulse mode operation is represented below.

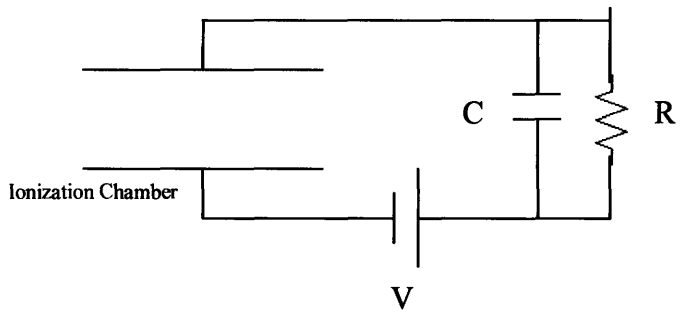

Figure 1.10 Circuit of ionization chamber operated in pulse mode.

In pulse mode, the signal voltage is the voltage measured across the load resistance. Prior to exposing the ion chamber to radiation, all the applied voltage is across the chamber and the voltage across the load resistance is zero. Once a radiation quantum enters the chamber's sensitive volume and ionization occurs, the ion pairs drift toward the corresponding electrode. The charge induced on the electrodes causes the voltage across the ion chamber to decrease. The voltage lost across the chamber is displaced across the load resistance. Thus, the pulse that occurs when incoming radiation interacts inside the chamber is a representation of the increase in voltage across the load resistance.

Current Mode

Current mode measures the total charge produced when the ion chamber is exposed the ionizing radiation. In other words, the average rate of ionization in the

chamber is determined. Unlike pulse mode, current mode is effective for detecting incoming radiation when event rates are very high because the individuality of the pulses is no longer important. In current mode, the time average of the current produced by many radiation interactions is measured. The circuit for current mode operation is represented below.

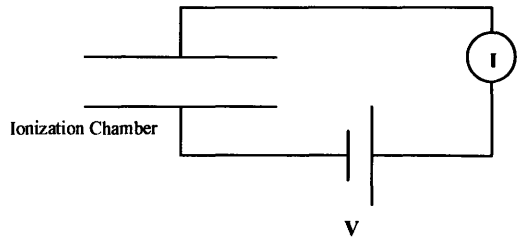

Figure 1.11 Circuit of ionization chamber operated in current mode.

In detail, prior to radiation exposure, the current across the chamber is equivalent to the voltage applied divided by the resistance across the chamber (via Ohm's Law).

$$I = \frac{V}{R} \qquad \text{Equation 1.8}$$

If the resistance across the chamber is large, then the current will measure approximately zero. When ionizing radiation enters the chamber's sensitive volume and ion pairs are formed, they drift toward the respective electrode. The drift of charge creates a current. The time average of that current is recorded in current mode operation.

1.5.3 Fast Neutron Detection Applicability

The detection medium for ionization chambers can be a solid, liquid, or gas. Conventionally, gas and superconductor materials have been used as the detection mediums, but noble gases in liquid phase have also been used since they are condensed dielectrics which allow electrons to remain free. The liberty of these electrons is important because it counteracts the affects of recombination. The consequences of using liquefied noble gases are the addition of refrigeration systems to maintain cryogenic temperatures and the achievement of sufficient purification of the liquid to eliminate

electronegative impurities. To avoid the hassle and expense of a refrigeration system, replacing the liquefied noble gases with non-polar liquids is proposed. Non-polar liquids operate like liquefied noble gases, but can be used at room temperature. However, the issue of purification still requires careful attention. These liquids have the benefit of being dielectric, dense, composed of primarily hydrogen, and fairly insensitive to gamma rays.

This thesis investigates the feasibility of employing an ionization chamber, filled with dielectric liquid, to detect fast neutrons with high efficiency and low cost. The three dielectric liquids that will be used for experimentation are tetramethylsilane (TMS), tetramethylpentane (TMP), and Isooctane.

1.6 Scope of this Study

The goal of this work was to ascertain whether a liquid ionization chamber that exploits the properties of dielectric liquids can be used to detect fast neutrons. Three chambers with different geometries were designed and tested. The first was a parallel geometry chamber constructed out of a polystyrene plastic called rexolite and grade 304 stainless steel plates. Rexolite is favorable because it has great dielectric properties, high voltage resistance, and good machinablilty. The second and third chambers were completely constructed with grade 304 stainless steel. The second was a cylindrical design and the third had parallel geometry.

As previously stated, the detection medium is dielectric liquid. These liquids must retain a high level of purity to successfully detect incoming neutrons; thus, a purification system was also designed and constructed. The liquids were cycled through the purification system, by pressure differentials, at least once before they were drained into the chamber. The purification can be monitored through several methods. One method involves analyzing electron lifetimes using the time-of-flight principle. A second method measures the signal height generated by detected particles and then compares it to the maximum attainable signal height. The maximum attainable signal height occurs in the case of an infinite electron lifetime.

The main objectives of this research are to design and construct three ionization chambers of different geometries, design and construct a dielectric liquid purification

system, detect neutrons generated from a 1Ci ^{238}Pu-Be source, and comparatively assess the advantages and shortcomings of each chamber.

Following the attainment of these goals, subsequent work would be to add more complex features (i.e. a grid, multi-electrode configurations, etc.) to the detector designs to improve efficiency and increase application compatibility.

1.7 Outline

Chapter 1 introduces the purpose and goals of this thesis. Chapter 1 also presents background information about neutron detection as well as the applications and limitations of current neutron detectors. Chapter 2 provides an explanation of the various components of this project. Detailed descriptions of the ionization chambers and purification system are given. In addition, the theory driving this research is presented. Chapter 3 provides an account of the purification process and purity monitoring. Chapter 4 presents the procedures and results of the x-ray exposure and the neutron exposure experiments. Chapter 5 is a discussion of the experimental results obtained. In addition, Chapter 5 renders a summary of the successes and shortcomings of this work and offers suggestions for future exploration.

Chapter 2

Room Temperature Dielectric Liquid Ionization Chamber

Until this thesis work, room temperature (dielectric) liquid ionization chambers had not been studied to detect fast neutrons, but they had been used to detect charged particles in other applications. For example, these chambers were used as calorimeters in high energy particle physics [9] and as monitors in radiation therapy [10]. The constructions of the chambers vary, but the common denominator is the use of dielectric liquids.

2.1 Dielectric Liquids

While dielectric liquids have been around for many years, their electronic properties were not studied until the late 1960s. There is currently a variety of known dielectric liquid compositions. This work examines three - TMS, TMP, and Isooctane. Table 2.1 features a list of dielectric liquids that can be used in the applications previously mentioned. The table also includes a list of their important properties.

Table 2.1 List of dielectric liquids and their important properties

Dielectric Liquid	Molecular Formula	Density (g/cm^3)	Molar Weight (g)	Dielectric Constant	Boiling Point (°C)	Melting Point (°C)	$\Delta E/\Delta x$ ($MeV/g\ cm^2$)
Tetramethysilane (TMS)	Si(CH3)4	.651	88.3	1.92	27	-100	2.04
Tetramethylpentane (TMP)	C9H20	.72	128.3	1.98	123	-67	2.15
Tetramethylgermanium (TMG)	Ge(CH3)4	1.006	132.8	2.01	43	-88	1.77
Isooctane	C8H18	.69	114.22	2.20	98	-107	-
Neopentane	C5H12	.613	72.1	1.84	9	-16	2.21

2.1.1 Benefits of using Dielectric Liquids to Detect Fast Neutrons

Various properties of dielectric liquids make them extremely attractive for use in fast neutron detectors. In Chapter 1, the challenges involved in detecting fast neutrons are discussed. Theoretically, these liquids appear to positively address each challenge; resulting in improved detection efficiency.

Gamma Insensitivity

Gamma contamination is continuously an issue when detecting fast neutrons. A current approach to dealing with this problem is neutron-gamma discrimination. The discrimination process is done by various methods including pulse shape analysis, 10% - 90% risetime measurements, time of flight, and figure of merit. The dielectric liquids under investigation provide an alternate solution for gamma contamination. In an ionization chamber, gamma rays are detected when Compton (incoherent) scattering occurs. Compton scattering is when gamma rays interact with the electrons of an atom in the target material and set a detectable electron free. Inherently, dielectric liquids are essentially gamma blind because the cross section for incoherent scattering in these liquids is extremely low. Figures 2.1, 2.2, and 2.3 illustrate the cross sections of incoherent scattering for hydrogen, carbon, and silicon for various photon energies. The data is normalized in order account for the ratios of each element within the molecule.

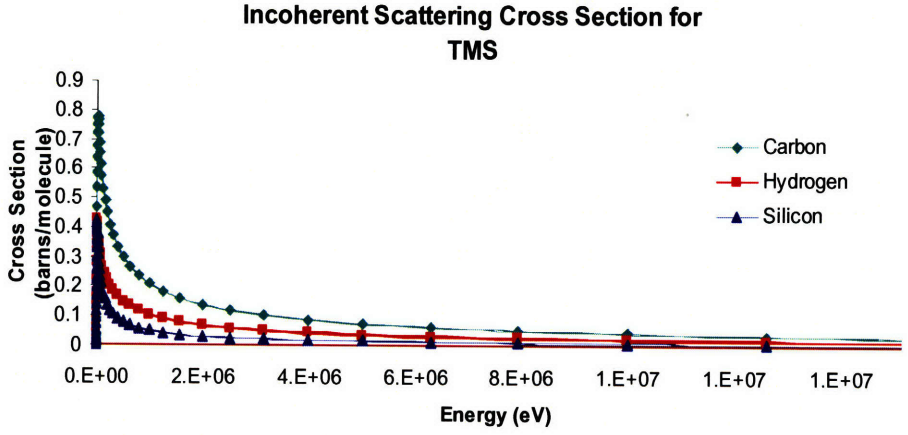

Figure 2.1 Incoherent scattering cross sections for hydrogen, carbon, and silicon target media at various photon energies for TMS.

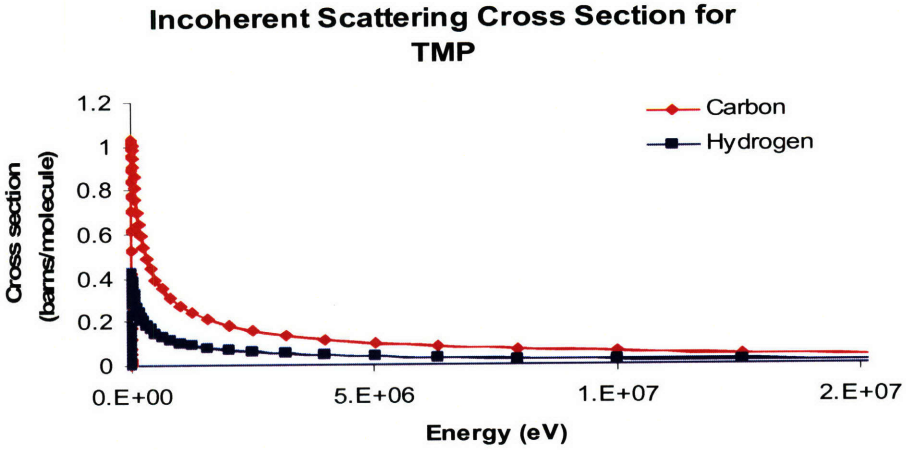

Figure 2.2 Incoherent scattering cross sections for hydrogen, carbon, and silicon target media at various photon energies for TMP.

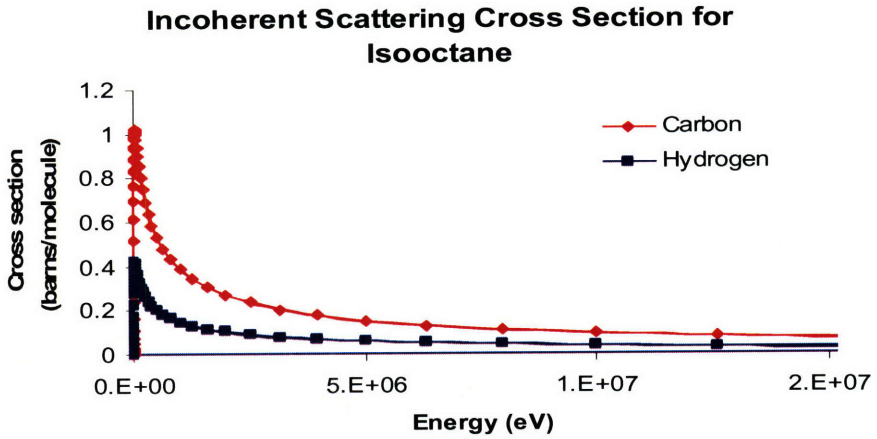

Figure 2.3 Incoherent scattering cross sections for hydrogen, carbon, and silicon target media at various photon energies for Isooctane.

Based on Figures 2.1, 2.2, and 2.3, incoherent scattering only appears to be an issue when low energy gammas are present. Shielding against those gammas with lead blocks should be an adequate solution.

Decreased Recombination

As discussed in Chapter 1, recombination is when an electron and a hole interact and neutralize each other. This is a problem if the electron-ion pair recombines after a

fast neutron ionizes them. The process of recombination causes the efficiency of the detector to be low because fast neutrons that are present cannot be detected. In ionization chambers, a sufficiently high electric field can minimize recombination. Since dielectric liquids are placed in between the chamber electrodes, the chamber can withstand high applied voltages. Another benefit of dielectrics is that when electric charges travel through them, the interaction energies and forces between the charges are reduced. This attribute discourages recombination.

High Density

High density is an advantageous quality in a fast neutron detector. Higher densities allow for thinner detectors, higher energy resolution, and higher efficiency. Gas detectors have low efficiency as a result of atoms being spread apart. The densities of substances are typically a factor of 10^2 to 10^3 larger in their liquid phase than in their gaseous phase. Consequently, the fast neutron detection efficiency would presumably be higher when liquid detection media, rather than gas, is used.

Fast Response

When electrons and ions in an ionization chamber are in the presence of an electric field, they migrate toward the oppositely charged electrode. As a result of the mass difference between the electrons and ions, the electron mobility is much faster than that of the ion. Most of the detection methods discussed in Chapter 1 are concerned with the detection of the ion or recoil proton. In ionization chambers, one has the choice of detecting the electrons, ions, or both. For the fastest response, it would make sense to only detect the electrons. This is done by implementing a shorter collection time than that necessary to detect ions.

Hydrogenous Composition

Hydrogen is the ideal elastic scattering nucleus when attempting to detect fast neutrons because fast neutrons transfer between 0 and 100 percent of their total kinetic energy to the hydrogen nucleus during a collision. The maximum transfer of kinetic energy is desired because it reduces the possibility of multiple neutron scattering. For

theoretical purposes, the kinetic energy transfer is generally averaged to 50 percent of the incoming neutron energy.

In typical plastic and liquid scintillators, the hydrogen/carbon (H/C) ratios are roughly 1:1, but in the dielectric liquids under investigation, the ratios are upward of 2:1. For example, TMP is 2.245:1 and Isooctane is 2.25:1. This implies that detectors filled with dielectric liquid will be more efficient neutron detectors than plastic and liquid scintillators.

Thermal Neutron Insensitivity

This work is only concerned with detecting fast neutrons, but thermal neutrons can be produced after an elastic scattering or backscattering event. When the goal is to detect fast neutrons, these thermal neutrons are considered unwanted background radiation. Fortunately, thermal neutrons do not have enough energy to ionize an atom in the dielectric liquids. As a result, they will not be detected in a detector based on elastic scattering. However, if the thermal neutrons create a charged particle (specifically an electron) by means other than ionization, the detector is no longer immune to thermal neutrons.

2.1.2 Safety Information

The benefits of dielectric liquids are many, but working with the ones under consideration requires safety precautions. They are extremely flammable in the liquid and vapor phase and can be hazardous to skin, eyes, and the respiratory system. The safety equipment that should be used when handling the liquids includes safety goggles, protective clothing, and gloves. In addition, the liquids should always be handled under a chemical fume hood and they should be stored in a tightly closed container away from open flames and sparks.

In the case of accidental inhalation, ventilation and/or oxygen should be accessed immediately. If the liquids come in contact with the skin or eyes, the affected area should be flushed for about 15 minutes. Clothing that is contaminated by the liquids should be immediately removed and washed. If swallowed, the mouth should be rinsed and a physician should be contacted without delay.

The liquids are colorless and smell like gasoline. The consistency of the liquids can be described as oily. If spilled on work tables, flooring, or other objects, the liquids can be sufficiently cleaned up with soap and water.

2.1.3 Purity Limitations and Monitoring

The purity of the dielectric liquids is extremely important for successful fast neutron detection. If the liquids are not adequately pure, electron trapping can occur. Electron trapping ensues when impurities in the liquid attach themselves to free electrons that are intended for detection.

Dielectric liquids are typically sold commercially with a purity specification of between 99.0 and 99.7 percent, depending on the liquid. However, once the liquids are exposed to air, they become contaminated with oxygen and other impurities. Since the liquids must be exposed to air before they are deposited into the chamber, they must be re-purified. A purification system was constructed to perform this task. The purity required for our purpose is discussed in Chapter 3.

For this application, the purity is generally discussed in terms of the electron lifetime in the dielectric liquid. The electron lifetime is the time that a free electron stays free. In an ideal pure liquid, the free electrons would have an infinite lifetime. The electron lifetime can be represented by Equation 2.1

$$\tau = \frac{1}{k \times [s]} \qquad \text{Equation 2.1}$$

where τ is the electron lifetime, k is the rate constant for the impurity attachment process, and [s] represents the concentration of electron-attaching impurities.

Purity monitoring methods are discussed in Chapter 1, but those methods typically require a grid or radiation source inside the chamber. Since neither was included in the chamber designs explored in this work, the purity was monitored by measuring the current across the chamber and calculating the conductivity. In a pure state, the dielectric liquids are perfect insulators and have an intrinsic conductivity less

than 10^{-18} $\Omega^{-1}cm^{-1}$. Applying high voltage across the chamber after it is filled with dielectric liquid further purifies the liquid.

2.2 Purification System Design

There are different techniques for purifying the dielectric liquids. In general, they are passed through molecular sieves and *Oxisorb* to remove impurities. Molecular sieves are similar to common filters, but they operate on a molecular level. The sieves contain tiny pores of precise sizes that absorb molecules of a corresponding size. *Oxisorb* absorbs oxygen molecules.

The purification system designed for this project is constructed of majority stainless steel. The material choice was based on cleanliness, low cost, and ease of use. A stainless steel container is used to hold the liquid while it is heated to vapor phase. The heating source is an electrical heating tape controlled by a Variac. The vapor is then passed through two types of molecular sieves – 4A and 13X, *Oxisorb,* and then into the chamber by pressure differentials. To create the pressure differentials, the system includes an "oil-free" roughing pump (Drivac, BH2-60HD). Argon is circulated through the system to isolate the *Oxisorb* from air. The Argon flow also assists in purging the system of any air that may have entered through tiny leaks. The heat exchanger has cooling water flowing through it and it is used to condense the vapor before filling the chamber. The inside tubing is stainless steel and the outside tubing is copper. The copper never comes in contact with the dielectric liquid. A heating tape is also placed around the molecular sieve container to sustain the vapor phase through the sieves and *Oxisorb*. The entire heating leg of the system s covered with high temperature insulation to assist in maintaining vapor phase flow. The system includes a check valve to restrict the directional flow and a Pressure Relief Valve (PRV) to constrain pressure. Figure 2.4 is an illustration of the purification system used for this work. Figure 2.5 is a photograph of the purification system.

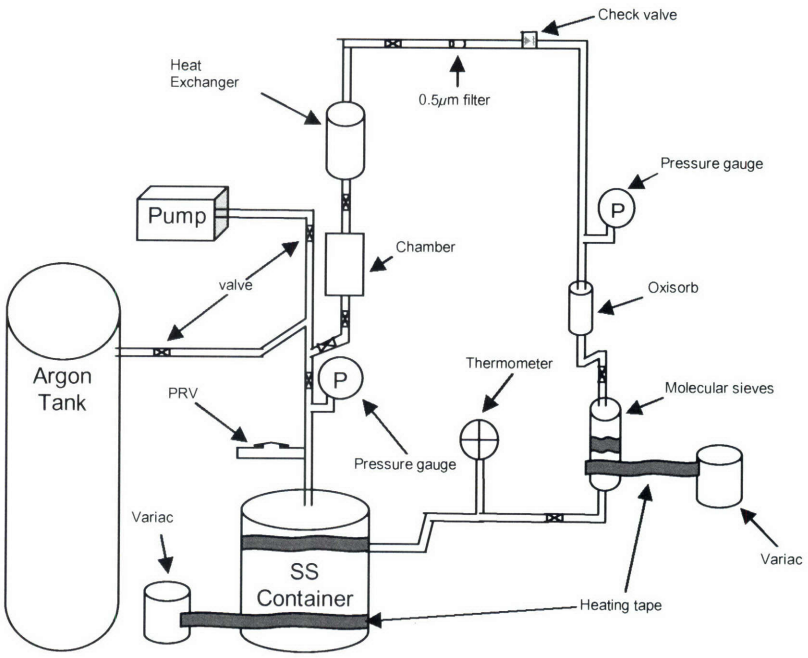

Figure 2.4 Schematic drawing of dielectric liquid purification system.

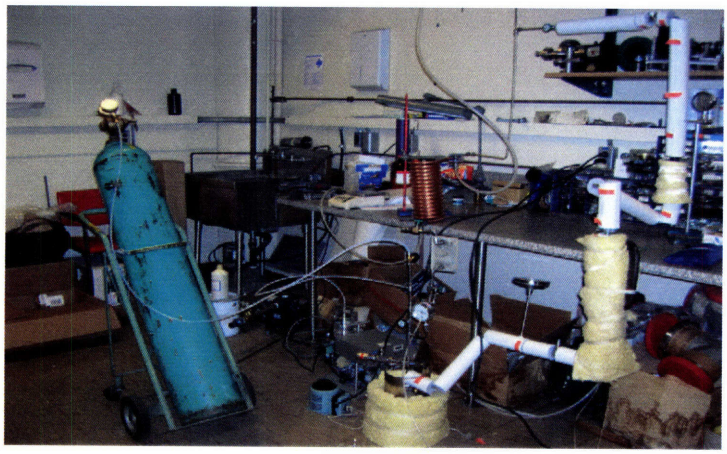

Figure 2.5 Photograph of dielectric liquid purification system.

2.3 Liquid Ionization Chamber Designs

As discussed in chapter one, three ionization chambers were constructed to investigate the feasibility of detecting fast neutrons using an ion chamber filled with room temperature dielectric liquid. Two of the chambers were constructed with parallel

plate geometry and the other with cylindrical geometry. The different geometries were investigated in order to observe how geometry influenced detection capabilities. Although the two of the chambers exploit the same geometry, they are constructed of different materials. In addition, the plate formation differs between the two.

2.3.1 Chamber 1

The first chamber was made out of Rexolite and stainless steel plate electrodes. The chamber consists of three parts that are sealed together with a dielectric epoxy (Axson RE12421). Screws are used for mechanical reinforcement. Figure 2.6 is a photograph of the chamber parts and Figure 2.7 is a photograph of the chamber after it is assembled and sealed.

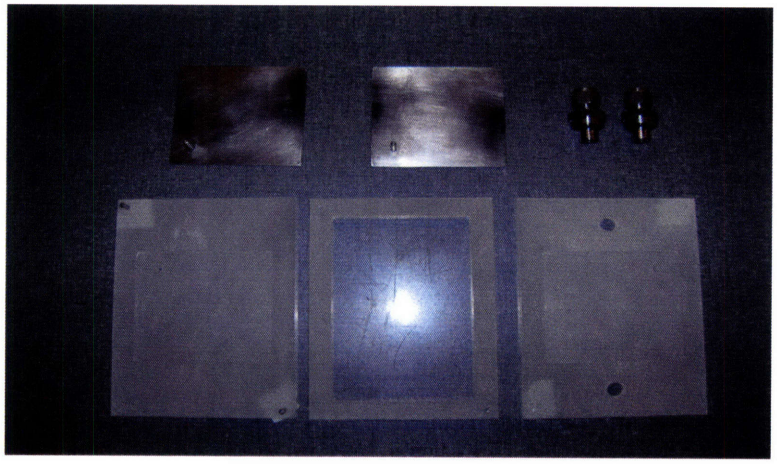

Figure 2.6 Photograph of chamber 1 prior to assembly

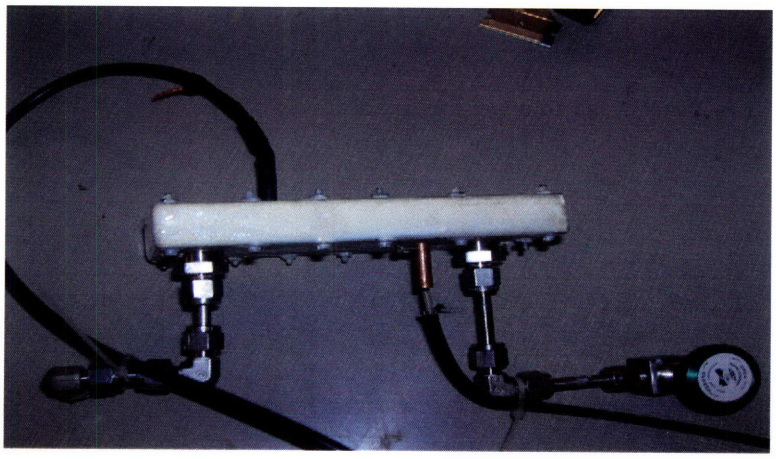

Figure 2.7 Photograph of chamber 1 after assembly

The dimensions of the chamber are 12.8cm x 8.4cm x .8cm and the dimensions of the electrode plates are 3in x 3in. The electrodes are separated by .5 cm. The sensitive volume of this chamber is 29cm^3 (see Appendix B). Copper posts are attached to the plate electrodes and coaxial cable is soldered to those posts. The coaxial cable is connected to the electronics.

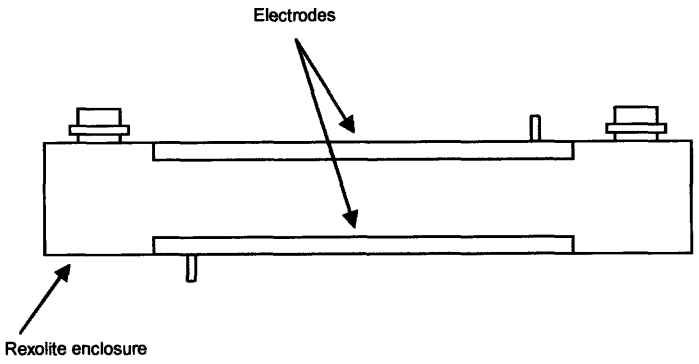

Figure 2.8 Cross-section view of chamber 1.

2.3.2 Chamber 2

The second chamber (cylindrical geometry) was constructed entirely out of stainless steel. The body of chamber was about 27cm long and 3 cm in diameter. A SHV electrical feedthrough serves as one endcap and a 2.75 inch diameter blank flange serves as the other endcap. A 7/8 inch stainless steel tube was attached to one side of the blank flange and a .12"(OD)/.10"(ID) stainless steel tube was attached to the electrical feedthrough. Once constructed, the 7/8 inch tube functioned as the cathode and the .12 inch tube functioned as the anode. The sensitive volume of this chamber is 70cm^3 (see Appendix B). Two stainless steel guard rings were also incorporated in the design. They were insulated from the electrodes with alumina ceramic. Figure 2.9 is a schematic drawing of the ion chamber cross section. Figure 2.10 is a photograph of the chamber parts and Figure 2.11 is a photograph of the chamber after assembly.

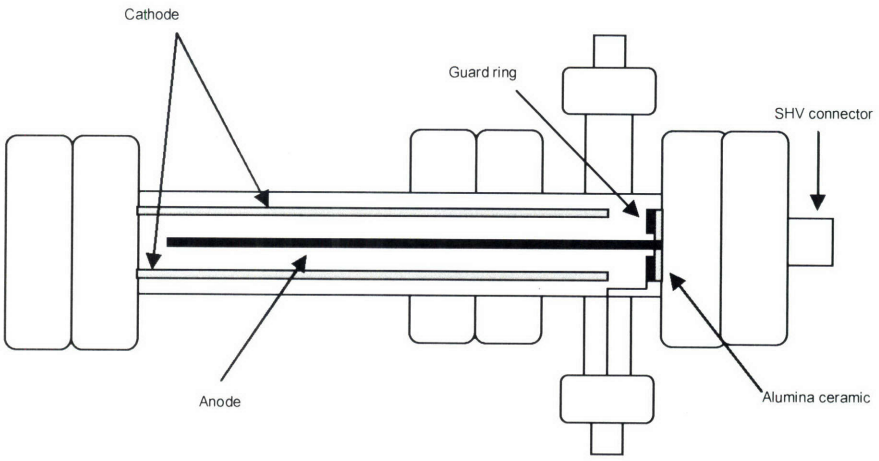

Figure 2.9 Cross-section view of cylindrical ionization chamber (chamber 2).

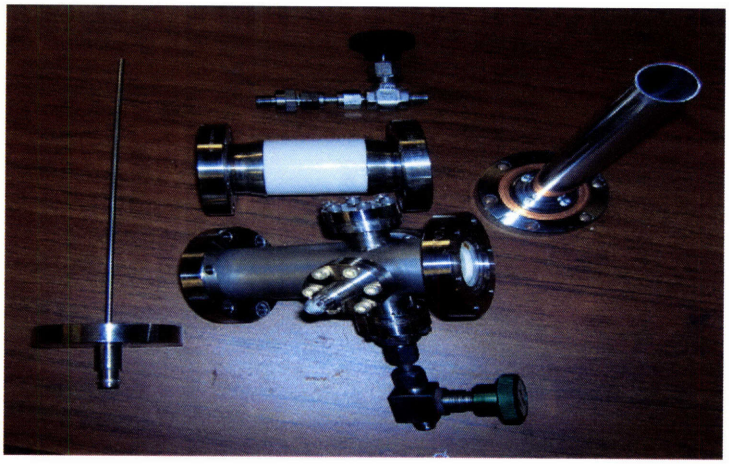

Figure 2.10 Photograph of chamber 2 parts prior to assembly

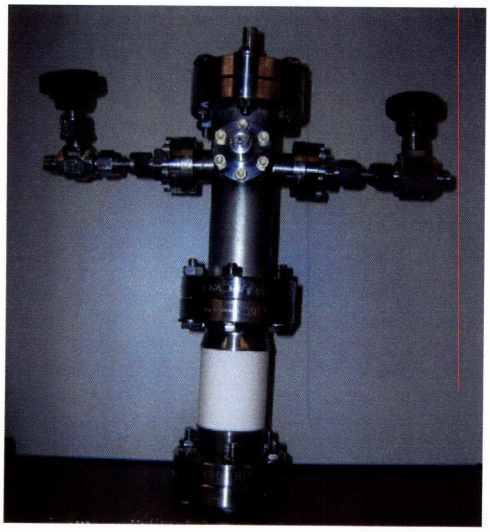

Figure 2.11 Photograph of chamber 2 after assembly

2.3.3 Chamber 3

The third ion chamber was constructed entirely of stainless steel. The design consists of two 6 inch flanges and one 6 inch spacer flange. The inside diameter of the spacer flange is 4 inches. The flanges are sandwiched together with the spacer flange in the center. Inside the chamber, a circular plate of 7/16 inch thickness and 3.3 inch diameter is placed on 5mm alumina posts. The separation distance between the center plate and the top/bottom flange is 5mm. The sensitive volume of this chamber is 55.15cm^3 (see Appendix B). The inside of the spacer flange is lined with a .78 inch tall (100mm outer diameter / 95mm inner diameter) tube of quartz glass. The purpose of the quartz glass is to insulate the anode from the inner chamber side-wall. The addition of the quartz tube is important because we only want to detect particles that travel along the uniform electric field lines between the top flange and the anode or between the bottom flange and anode. The chamber has two ports for filling and a SHV connector for supplying high voltage. Figure 2.12 is a schematic drawing of the ion chamber cross section. Figure 2.13 is a photograph of the chamber parts and Figure 2.14 is a photograph of the assembled chamber.

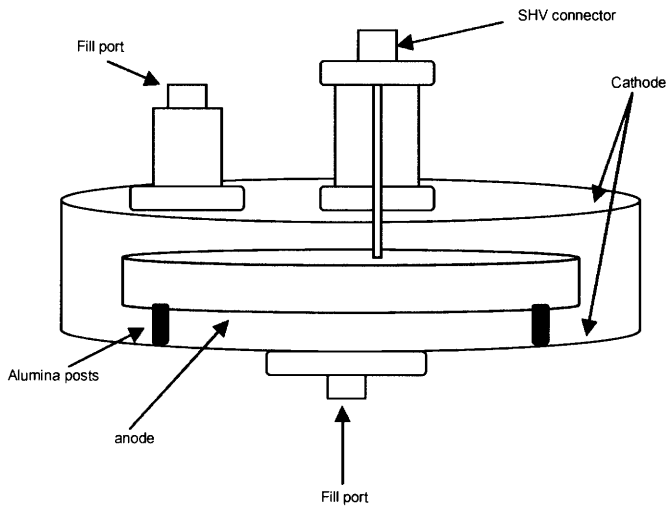

Figure 2.12 Cross-section view of chamber 3.

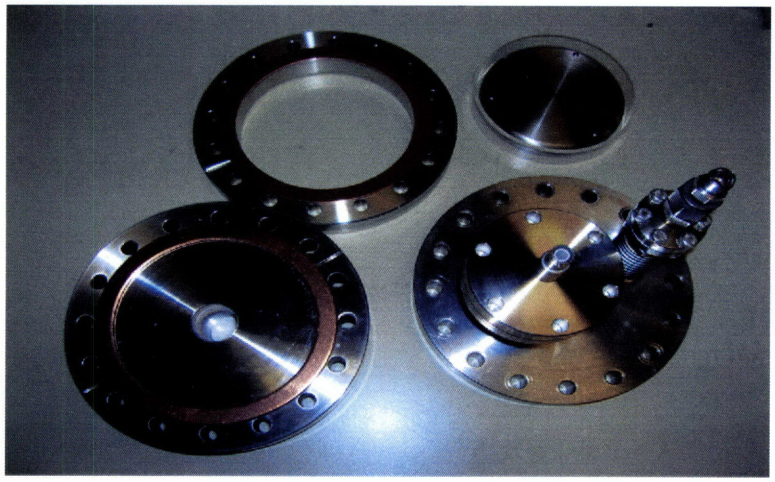

Figure 2.13 Photograph of chamber 3 parts

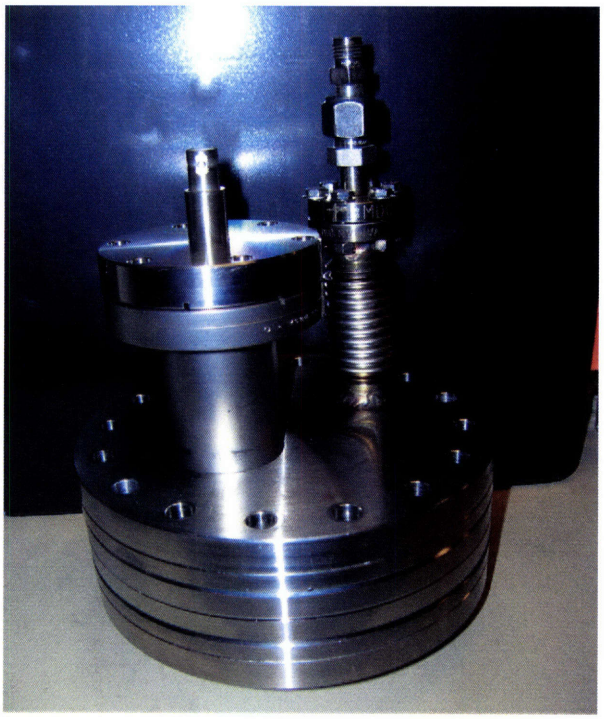

Figure 2.14 Photograph of chamber 3 assembled (screws added later)

2.4 Electronics

The electronics setup for the first chamber consists of a high voltage supply (Bertan, model 1792N) connected, through a 10 MΩ resistor, to one plate electrode in the

chamber. The other plate is grounded through a 100,000 Ω resistor. The signal from the charge collection is received by a charge sensitive preamplifier (Cremat, CR-110) that is inserted into a test board (Cremat, CR-150). The test board assists in evaluating the preamplifier. The gain of the preamplifier is 1.4 V/pC. A power supply (Acopian, DB-12-10) is connected to the test board. From the preamplifier, the signal is read to an amplifier, then to an oscilloscope. The chamber is placed inside a steel enclosure in order to reduce noise. Figure 2.15 is a schematic drawing of the electronics and Figure 2.16 is a photograph of the preamplifier, test board, and power supply.

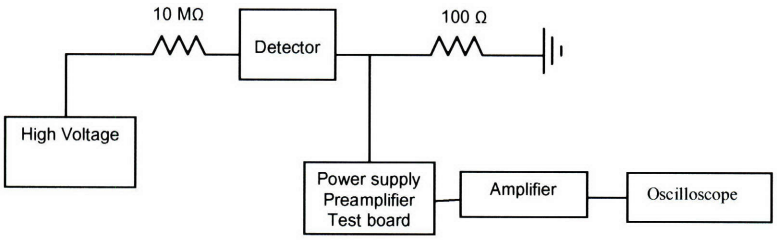

Figure 2.15 Schematic drawing of electronics.

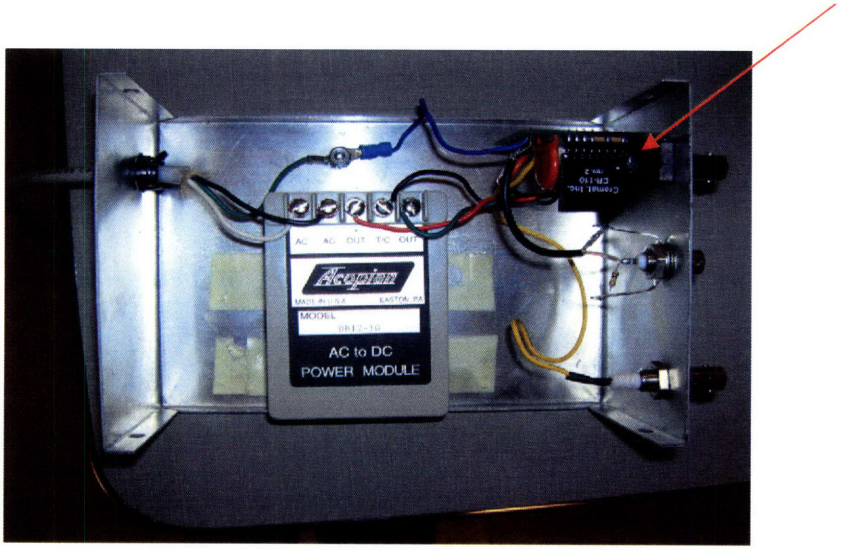

Figure 2.16 Photograph of electronics

The electronic setup used for the two stainless steel ion chambers was slightly different. High voltage was supplied to the detector through a low noise preamplifier with conversion gains of nominally 47 mV/M-ion-pairs (Canberra, model 2006). The

output signal, read from the same preamplifier, was sent to an amplifier (Ortec, model 471). The signal was observed with an oscilloscope. The change in electronic setup was not motivated by any problem with the previous setup. In theory, the electronic setups can be used interchangeably.

2.4.1 Electronic Noise

Electronic noise is a characteristic inherent of all electrical circuits that causes the unwanted effect of obscuring the detection of a valuable signal. In this work, the signal-to-noise ratio is a significant concern because the amplitudes of the signals detected are low (see Appendix A). If the noise amplitude is substantial, the detected signal is overwhelmed by the noise and rendered unreadable.

Common sources of noise are ground loops, transmitted noise from external sources, and the inherent noise of electronic components. To reduce the noise in our system, a low noise preamplifier was exploited and ground loops were avoided. In addition, shielding was placed around all non-metal components of the detector. The shielding used was either aluminum or steel. For chambers 2 and 3, the chamber enclosures themselves functioned as shielding. Chamber 1 was placed inside a steel box for shielding.

2.5 Theory

The theory involved in analyzing the success of this fast neutron detection method consists of cross section, pulse height, and efficiency analysis. Each analysis was performed before the experimental work began. The theory only considers the three dielectric liquids that were investigated in this work – TMS, TMP, and Isooctane.

2.5.1 Cross Section Analysis

It is important to consider the interactions that can happen in each of the dielectric liquid media when a fast neutron is present. TMS has a molecular formula of $(CH_3)_4Si$;

thus, the neutron can react with hydrogen, carbon, or silicon nuclei. The other two liquids used in this work are composed of only hydrogen and carbon. The molecular formula of TMP is C_9H_{20} and C_8H_{18} for Isooctane. The cross sections at various neutron energies give us information about which reactions are most likely.

Figures 2.17, 2.18, and 2.19 illustrate the cross sections of the dominant competitive processes for hydrogen, carbon, and silicon. The data in Figure 2.17, 2.18, and 2.19 are normalized in order to account for the ratios of each element within the molecule.

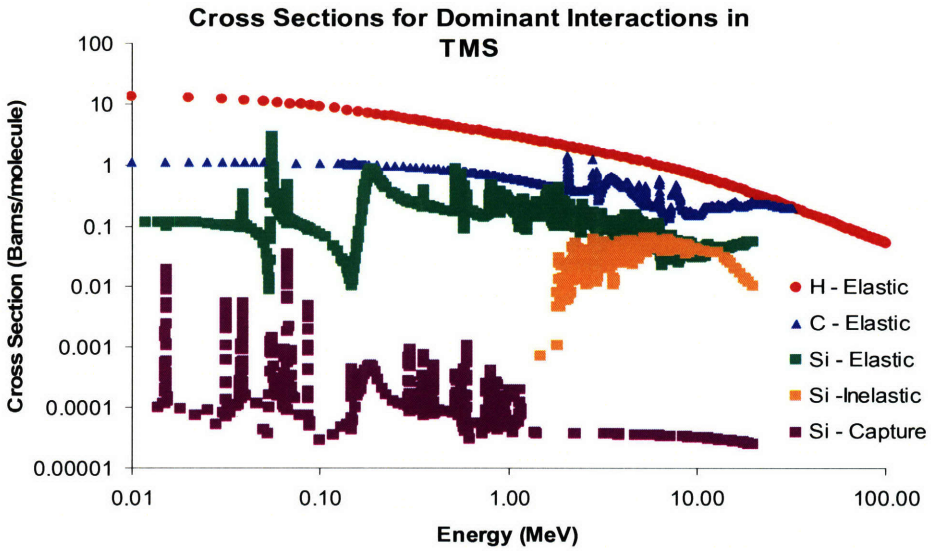

Figure 2.17 Graph of cross sections data for dominant reactions in TMS (log scale).

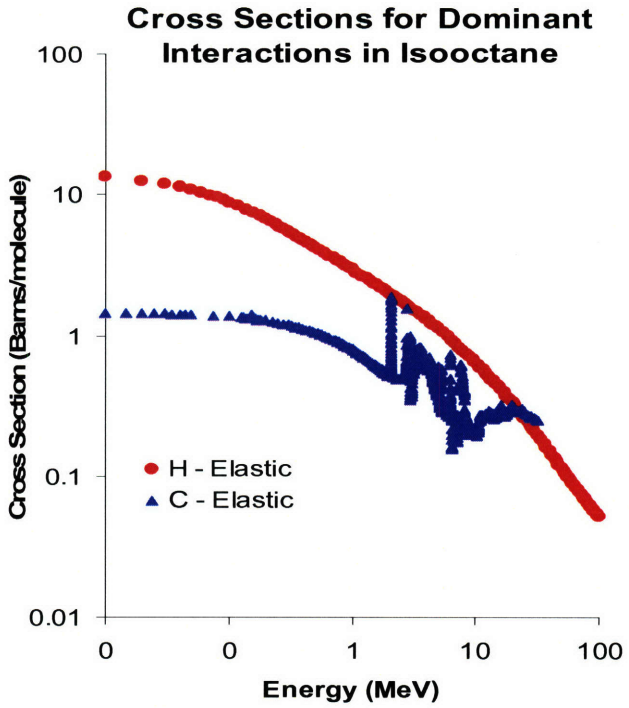

Figure 2.18 Graph of cross sections data for dominant reactions in Isooctane (log scale).

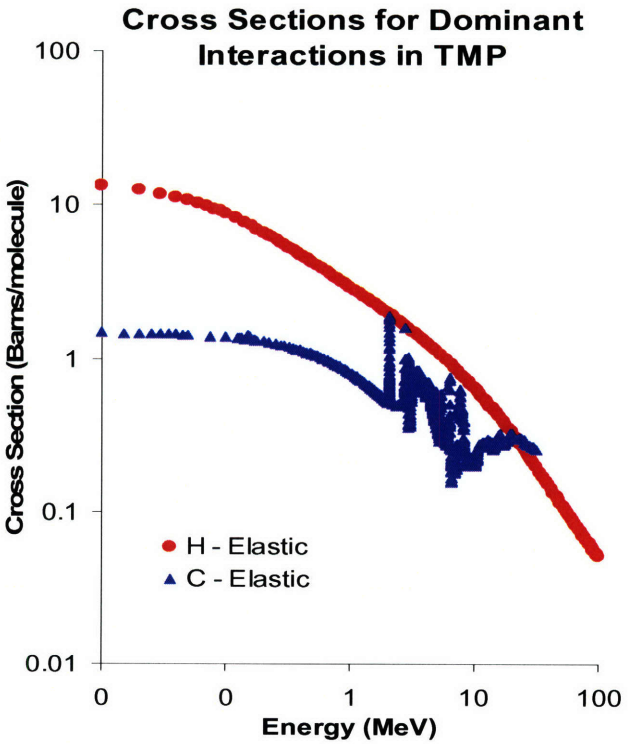

Figure 2.19 Graph of cross sections data for dominant reactions in TMP (log scale).

It appears that elastic scattering off silicon, hydrogen, and carbon nuclei is similar in likelihood. However, it is important to remember that there is a higher ratio of hydrogen in each liquid. The elastic scattering interaction off hydrogen is the most desired because of the likelihood of a full energy transfer. The ideal situation is for the neutron to interact with a target nucleus and loose all of its energy. If the neutron has a moderated energy after the first collision, which is the case when the first collision is with a carbon or silicon nucleus, then it can interact again. This presents a problem because multiple scattering may produce unwanted detection.

2.5.2 Pulse Height Analysis

The detection process begins with the neutron passing through the chamber and interacting with a target nucleus in the liquid medium. This interaction initiates the production of an ion pair. The applied electric field causes the positive ion to drift toward the negatively charged plate and the electrons to drift toward the positively charged plate. Electrons are more mobile than positive ions so the electrons will drift to the appropriate plate much faster than the positive ion. Due to the slow mobility of positive ions, for this analysis, only the collection of the electron charge is considered for detection. In electron sensitive mode, the collection (sample) time is set to a value less than the time it takes for the positive ions to be collected; thus, only the electrons will have time to be collected. Every time an electron is collected on the positive plate, there will be a drop in the ion chamber voltage.

The amplitude for each pulse can be calculated using equation 2.2.

$$V_{electrons} = \frac{q_e x}{Cd} = \frac{nxe}{2Cd} = \frac{E_n xe}{4CWd} = \frac{E_n xeG_{tot}}{4C(100eV)d} \qquad \text{EQ. 2.2}$$

where q_e is electron charge, x is the distance between the positive plate and where the ion pair was formed, C is the capacitance, d is the distance between the plates, n is the number of ion pairs, e is electron charge, E_n is the initial neutron energy, W is the amount of energy (eV) lost by the incoming neutron, and G_{tot} is the total number of electrons released per 100eV of deposited energy (W/100eV).

Our calculation of $V_{electrons}$ for an incoming neutron with energy of 4.5 MeV (average energy of a neutron from a ^{238}Pu-Be source) gave a value of 2.70mV, 2.88mV, and 1.65mV per pulse for TMS, TMP, and Isooctane respectively. The details of this calculation can be found in Appendix A.

2.5.3 Intrinsic Efficiency

The intrinsic efficiency of a detector is the number of radiation quanta detected out of the number of radiation quanta incident on the detector.

$$\varepsilon_{\text{int}} = \frac{\#of.radiation.quanta.recorded}{\#of.incident.radiation.quanta} \qquad \text{Equation 2.3}$$

The intrinsic efficiency depends on the detector material, radiation energy, and the thickness of the detector in the direction of radiation. There is also slight dependence on the distance between the detector and the radiation source.

TMP and isooctane are composed of hydrogen and carbon, while TMS has the addition of the silicon. Neglecting multiple scattering, the intrinsic detection efficiency is calculated using Equation 2.4.

$$\varepsilon = \frac{N_H\sigma_H}{N_H\sigma_H + N_C\sigma_C + N_{Si}\sigma_{Si}} \cdot (1 - e^{-d(N_H\sigma_H + N_C\sigma_C + N_{Si}\sigma_{Si})}) \qquad \text{Equation 2.4}$$

where N is the nuclear number density of the target nuclei, σ is the scattering cross section, and d is the pathlength through the detector for incident neutrons (detector thickness). The nuclear number density for hydrogen, carbon, and silicon was calculated using Equation. 2.5

$$N_x = \frac{n_x}{V_{dielectic}} \qquad \text{Equation 2.5}$$

where n_x is the number of hydrogen, carbon, or silicon atoms (x) in one molecule and $V_{dielectric}$ is the volume of one molecule of the particular dielectric liquid. $V_{dielectic}$ was calculated using Equation 2.6

$$V_{dielectic} = \frac{m}{\rho} \qquad \text{Equation 2.6}$$

where m is the molar mass of the dielectric liquid divided by Avogadro's number, which is also the mass per molecule of dielectric liquid, and ρ is the density of the dielectric liquid.

When the neutron scatters off hydrogen, 0 to full neutron energy will be transferred to the recoil proton (estimated as one half of the full neutron energy). When the neutron scatters off carbon or silicon, the neutron will lose some energy and may contribute to multiple scattering events. In general, the neutron will lose between 0 and 28 percent of its initial energy to the recoil proton in a carbon scattering event. The calculated intrinsic efficiencies for TMP, TMS, and Isooctane are plotted in figures 2.20, 2.21, and 2.22 and Table E.1 (Appendix E).

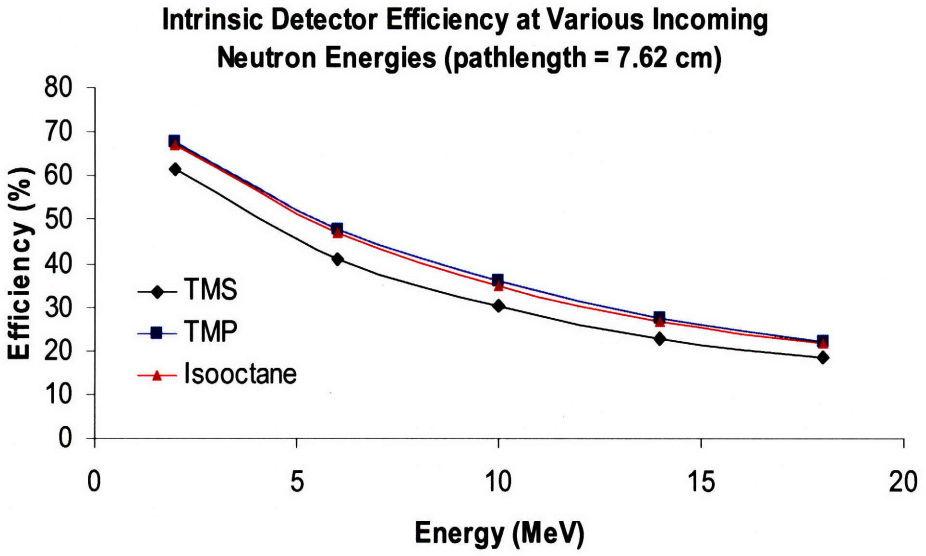

Figure 2.20 Calculated intrinsic detection efficiency of TMS, TMP, and Isooctane at various incoming neutron energies for the first chamber. The pathlength is 7.62 cm (3 inches).

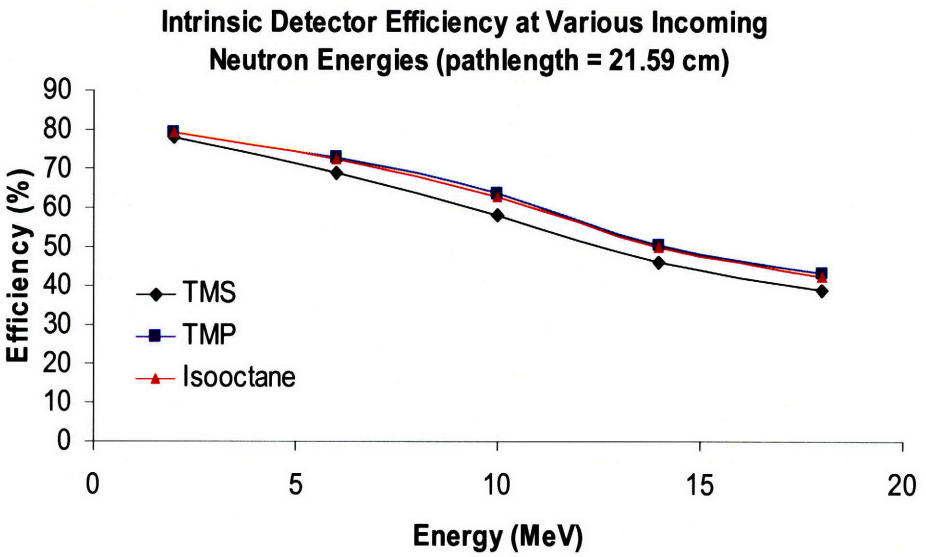

Figure 2.21 Calculated intrinsic detection efficiency of TMS, TMP, and Isooctane at various incoming neutron energies for the second (cylindrical) chamber. The pathlength is 21.59cm.

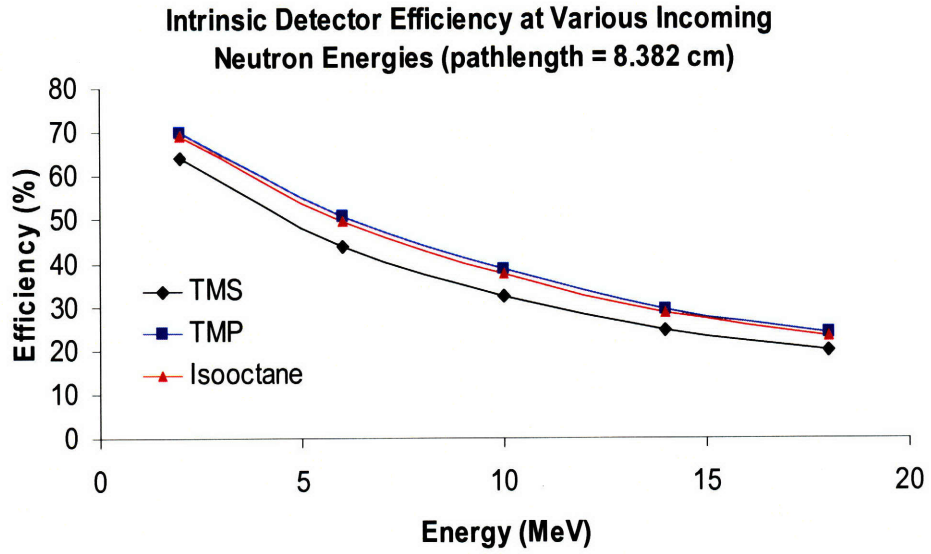

Figure 2.22 Calculated intrinsic detection efficiency of TMS, TMP, and Isooctane at various incoming neutron energies for the third chamber. The pathlength is 8.38 cm.

2.5.4 Absolute Efficiency

The absolute efficiency is the number of radiation quanta detected out of the number of radiation quanta emitted by the source.

$$\varepsilon_{abs} = \frac{\#of.radiation.quanta.recorded}{\#of.radiation.quanta.emitted.by.source} \qquad \text{Equation 2.7}$$

The absolute efficiency depends on the detector properties, geometry, and apparatus setup (distance between source and detector). The relationship between intrinsic efficiency and absolute efficiency is shown is Equation 2.8.

$$\varepsilon_{abs} = \varepsilon_{\text{int}}(\frac{\Omega}{4\pi}) \qquad \text{Equation 2.8}$$

In the above equation, Ω represents the solid angle in (units) steradians. The solid angle is the angle subtended by the detector. The solid angle, when measured in steradians, is

represented as the surface area of the face of the detector closest to the source divided by the distance between the source and the detector squared.

$$\Omega = \frac{SA}{d^2} \qquad \text{Equation 2.9}$$

In Equation 2.9, d is the distance between source and surface of the detector face and SA is the surface area of the detector face. The solid angles for each detector are calculated in Appendix D.

The calculated absolute efficiencies for TMP, TMS, and Isooctane can be found in figures 2.23, 2.24, and 2.25 and Table E.2 in Appendix E.

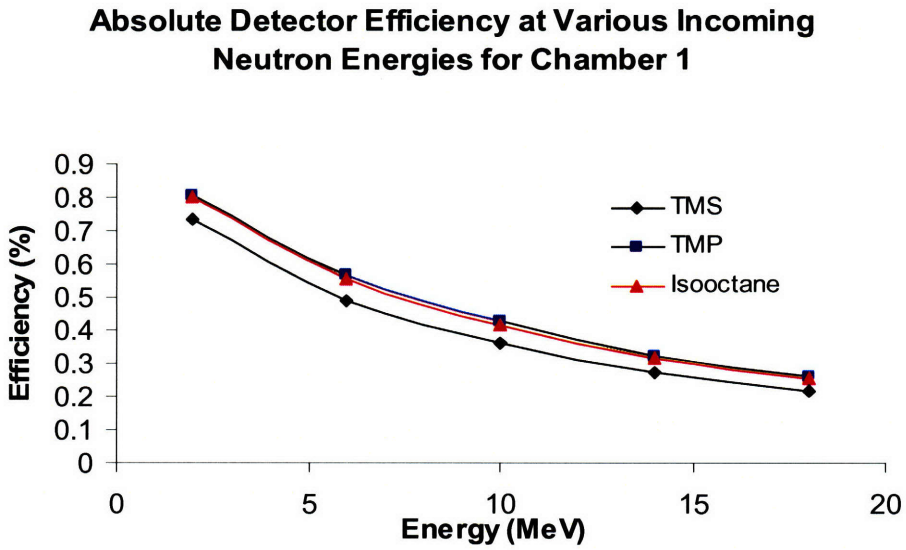

Figure 2.23 Calculated absolute detection efficiency of TMS, TMP, and Isooctane at various incoming neutron energies for chamber 1. The pathlength is 7.62cm and the solid angle was .15 steradian.

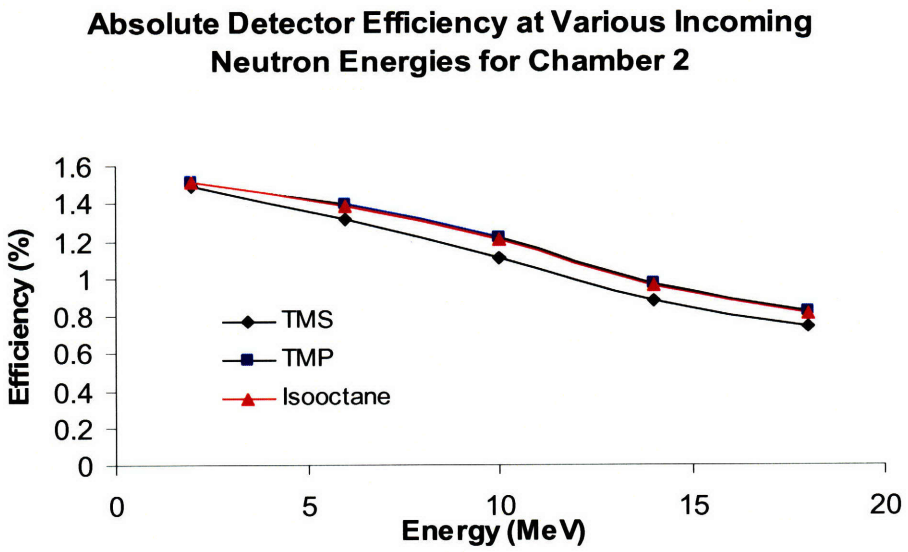

Figure 2.24 Calculated absolute detection efficiency of TMS, TMP, and Isooctane at various incoming neutron energies for chamber 2. The pathlength is 21.59cm and the solid angle was .24 steradian.

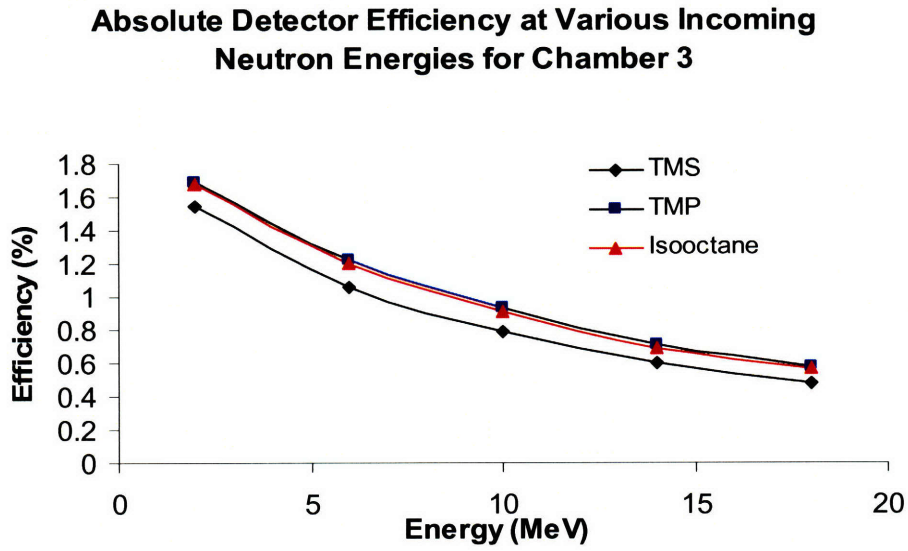

Figure 2.25 Calculated absolute detection efficiency of TMS, TMP, and Isooctane at various incoming neutron energies for chamber 3. The pathlength is 8.38cm and the solid angle was .31 steradian.

Chapter 3

Purification and Monitoring

Purifying the dielectric liquids is a process that is critical to the successful operation of the dielectric liquid fast neutron detector. Without sufficient purification, the detection efficiency is reduced because impurities combine with freed electrons before they can be detected. The purification process must be extremely efficient since contamination as small as 5 parts per billion is enough to combine with most of the freed electrons [11]. In general, the electron lifetime should be much greater than the electron's drift time in the chamber in order to collect the total charge produced.

In order to maintain the cleanliness of the liquids, the chamber and purification system must also be sufficiently clean, otherwise, the impurities present will contaminate the liquid. Thus, in addition to purifying the liquids, we have taken the precaution of cleaning the chamber and purification system. The procedures for the cleaning processes are further discussed in this chapter.

3.1 Purification Facility

Consideration must be given to the location where the liquids are purified. The safety measures that need to be taken into account when working with these liquids were discussed in Chapter 2. Ventilation, a water source (for flushing), and a fire extinguisher are features that must be present on site.

Our lab space was located in the basement of Building NW-13, room 067. The space offered a sink as a water source and a readily available fire extinguisher. The ventilation in the lab was less than perfect, but the doors were always left open, and the air conditioner was used to generate air flow.

3.2 Cleaning Purification System

The system is cleaned by first filling the stainless steel container with ethanol. The ethanol is heated to vapor phase and circulated through the system the same way the dielectric liquids are circulated – by pressure differentials. The boiling point of ethanol is 78.4 °C. Once ethanol has been circulated through the system and emptied into a separate container, an argon gas flow through the system is applied. The argon gas dries the molecular sieves and pushes remaining impurities out of the system. Argon is allowed to flow through the system for about 3 hours then the system is pumped down to roughly 5 mTorr using a roughing pump (Dryvac, BH2-60-5010). This pump provides oil-free pumping down to the 10^{-5} Torr range. The system is then closed and the pump is turned off. Next the heating tapes are turned on and the system is allowed to bake at 100°C for about 60 minutes. Baking the system assists in removing impurities from the inside walls of the tubing and other components. After the 60 minutes of baking, the pump is restarted. The system is evacuated and baked simultaneously for 8 hours. Afterward, the system is sealed and considered clean enough for our intent and purpose.

Purification systems used for purifying dielectric liquids can be cleaned in various ways, but a combination of pumping and baking is typically employed. The cleaning process used in another study evacuates the systems using a turbo-molecular pump while baking at 150°C for a few days [12]. Their evacuation was stopped at a pressure of 1.0 x 10^{-3} Pa (.0075 mTorr).

3.3 Cleaning the Chamber

All of the chambers we constructed were leak tested and cleaned before they were filled with purified dielectric liquid. First, all stainless steel chamber components were given an ethanol bath. The parts were allowed to air dry for a few minutes. Once sufficiently dry, the chambers were assembled and tested for leaks. The leak test was performed by filling the chambers with 30 PSI of argon glass and monitoring the pressure. The pressure was monitored for 24 hours. If the chamber remained at 30 PSI for 24 hours, the chamber passed the leak test. However, if leaks were present, *Snoop*®

leak detector was used to locate the leaks. Once the leaks were identified, they were sealed by adding epoxy or tightening bolts (depending on the chamber construction). The epoxy was only used on the chamber constructed with *Rexolite*. The two stainless steel chambers were sealed with copper gaskets and bolts. The leak-free chambers were then pumped down to 5 mTorr and baked at 100°C for about 8 hours.

Other methods for chamber cleaning have been exploited in previous research. One method consisted of an alkaline ultrasonic bath and subsequent rinsing with desalinated water [10]. Following the chemical cleaning, they rinsed the system with clean TMS. Finally, the chamber was dried in a ventilated oven. During this process, they filled and emptied the chamber about half a dozen times.

3.4 Purification Process

Once the chamber and the purification system are cleaned, pressure differentials are created in the purification system. The entire system is pumped down to approximately 10 mTorr and the chamber is pumped down to 5 mTorr. The valve uniting the chamber to the rest of the system is closed. The dielectric liquid, which is at atmospheric pressure, is drawn into the purification system as a result of lower pressure in the stainless steel container. The heating tapes attached to the stainless steel liquid and molecular sieve containers are then turned on and the liquids are heated to their boiling points. Maintaining vapor flow is also a concern because the vapor tends to condense in the purification system due to the low temperature in the laboratory environment. To rectify this issue, insulation and additional heating tapes are added to system when necessary. Once the vapor flows past the *Oxisorb,* the cooling water is turned on to encourage vapor flow toward the chamber. The cooling water flows through the heat exchanger, which is located directly before the chamber in the assembly. For illustration, a schematic drawing of the purification system is provided in Figure 2.4 in Chapter 2. As the vapor passes through the heat exchanger, it liquefies. The chamber valve is then opened and the liquid is sucked into the chamber as a result of the lower pressure. As soon as the chamber is full, the valves are closed the chamber is prepared for experimental use.

3.4.1 Difficulties

In general, the purification process worked well; however, there were a few complications that were encountered. First, chamber 2 and 3 were constructed entirely out of stainless steel which made it difficult to tell if the chamber was completely full. The suspicion of small bubble presence within the chambers is valid, but we are fairly confident that they are extremely small, if they exist at all. The behavior exhibited during the filling of the first chamber supports that belief. Chamber 1 is constructed out of *Rexolite*, which is relatively transparent. Therefore, the amount of liquid in the chamber can be visually observed. Chamber 1 successfully filled without any visible bubbles.

Another issue was maintaining the vapor phase of Isooctane and TMP. Both liquids have high boiling points, 98°C and 123°C respectively. To keep the vapor from condensing, the entire heating leg of the purification system must be kept at sufficiently high temperature. This requires the use of at least 3 heating tapes and adequate insulation.

3.5 Monitoring Purity

The purity of the liquids is characterized by the electron lifetime. A longer electron lifetime within the liquids, indicates better purity. Chapter 1 and 2 briefly discuss methods of monitoring purity. The methods discussed were the time-of-flight principle, signal height comparison, and conductivity comparison.

3.5.1 Time-Of-Flight Principle

Monitoring purity using the time-of-flight principle is a direct way of determining the electron lifetime by analyzing the current pulse generated in the chamber. Pulse shape analysis has been shown to be a proficient way of measuring electron lifetime [18] and [19].

Pulse Shape Analysis

An illustration of a pulse generated from the electrons and ions produced in an ionization chamber is given in Figure 3.1.

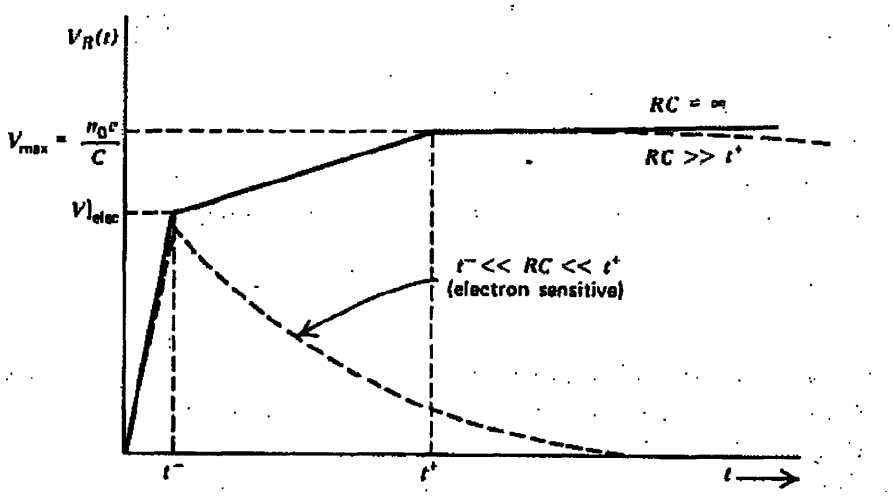

Figure 3.1 Output pulse shape from an ion chamber for various time constants [1].

During the time between 0 and t^-, the electrons travel to the anode. The time at which all the electrons reach the anode is t^-. At this point, the electrons no longer contribute to the amplitude of the signal. The pulse height continues to increase with time as the ions travel toward the cathode. Once the ions are collected (at time, t^+), the voltage no longer increases. The pulse rise time of the electrons is faster than that of the ions since electron velocity is much greater than ion velocity, especially with the liquids used in this study.

In this work, the detectors are run in electron-sensitive mode; thus, the ion contribution of the pulse is not considered. This pulse is also illustrated in Figure 3.1. The tail of the pulse is shown as a dotted line. The amplitudes of the pulses recorded in electron-sensitive mode are a function of the location at which the ion pairs were formed in the chamber. If the ion pair was created close to the anode, the electron has a shorter distance to traverse than if the pair was produced closer to the cathode. The shorter the electron travel time is, the smaller the voltage pulse. Likewise, a longer travel time produces a larger voltage pulse. This position dependence leads to a range of pulse heights even if the incoming radiation is monoenergetic.

The electron lifetime is determined with Equation 3.1 and 3.2.

$$\frac{Q_a}{Q_c} = e^{-\frac{t_d}{\tau}} \qquad \text{Equation 3.1}$$

Q_a is the charge at the anode, Q_c is the charge at the cathode, t_d is the electron drift time, and τ is the electron lifetime. Solving Equation 3.1 for τ, we get Equation 3.2.

$$\tau = \frac{-t_d}{\ln(\frac{Q_a}{Q_c})} \qquad \text{Equation 3.2}$$

The electron drift time is a function of the electrode separation distance and the electron drift velocity at operating conditions. It can be retrieved by examining the time between the beginning of the cathode and anode pulse. The charge at the anode and cathode is obtained from the amplitude of the pulses. If there were no impurities in the liquid, the electron lifetime would be 1 ($Q_a = Q_c$).

3.5.2 Signal Height Comparison

Measuring the signal height of the current pulse generated in the detector and then comparing that value to the maximum attainable signal is an indirect way of determining electron lifetime. The measurement is accomplished by exposing the detector to a source that produces electrons of known energy. The signal height from the detector is compared to what the signal height would be if the electron lifetime were infinite. Calculating the ratio of the two pulse heights is a quick and convenient way of determining electron lifetime. Equation 3.3 provides the electron lifetime as a percentage infinite electron lifetime.

$$\tau = \frac{chamber.signal.height}{\max obtainable.signal.height} \times 100 \qquad \text{Equation 3.3}$$

3.5.3 Conductivity

A feature of the dielectric liquids under investigation is that they are perfect insulators when they are pure. In their pure state, they have a very low conductivity of less than $10^{-18}\Omega^{-1}$ cm $^{-1}$. Conductivity is a measure of how well a solution conducts

electric current between oppositely charged electrodes. The conductivity of the dielectric liquids can be calculated by first calculating the resistivity. The relationship between resistivity and conductivity is shown in Equation 3.4.

$$\xi = \frac{1}{\sigma} \qquad \text{Equation 3.4}$$

ξ is the conductivity and σ is the resistivity. Resistivity is calculated from the resistance between the electrodes, distance between the electrodes, and area of the electrodes.

$$\sigma = \frac{AR}{x} \qquad \text{Equation 3.5}$$

A is the area of the electrodes, R is the resistance between the plates, x is the electrode separation. Resistance is calculated from Ohm's Law.

$$R = \frac{V}{I} \qquad \text{Equation 3.6}$$

R is the resistance, V is the voltage applied across the plates, and I is the measured current. Conductivity is measured in units of mho, in SI units in Siemens.

When using this method of determining purity, the conductivity of the chamber itself must be accounted for because the conductivity of the liquid alone is the value of sought after. This can be done by calculating the conductivity when the chamber is empty and when it is filled with dielectric liquid. The latter value can be subtracted from the former to determine the conductivity of the liquid.

3.5.4 Liquid Purity

Pulse shape analysis was used in this work to determine the purity of the dielectric liquids. To carry out this process, a small purity monitor was constructed. The purity monitor was essentially a parallel plate ionization chamber with a 1 μCi Americium-241 source attached to the cathode. This same method has been used to

monitor the purity of liquid detection media with ^{207}Bi and ^{210}Po sources [18], [19], [20]. However, most relatively pure beta and/or alpha emitters could be substituted as the radioactive source. Gamma and neutron sources are inadequate because their interaction location is uncertain. The shorter range of the alphas and betas make them more viable choices.

The outside of the chamber was made out of aluminum and the electrodes were copper plated zinc. The electrodes were circular with a diameter of about 2 cm. The plates were separated by about 2 cm and the monitor walls were isolated from ground with plastic spacers and o-rings. The chamber was shielded with heavy duty aluminum foil. Negative voltage was applied to the cathode and positive voltage was applied to the anode. An illustration of the purity monitor is shown in figure 3.2 and figure 3.3 is a photograph of the chamber.

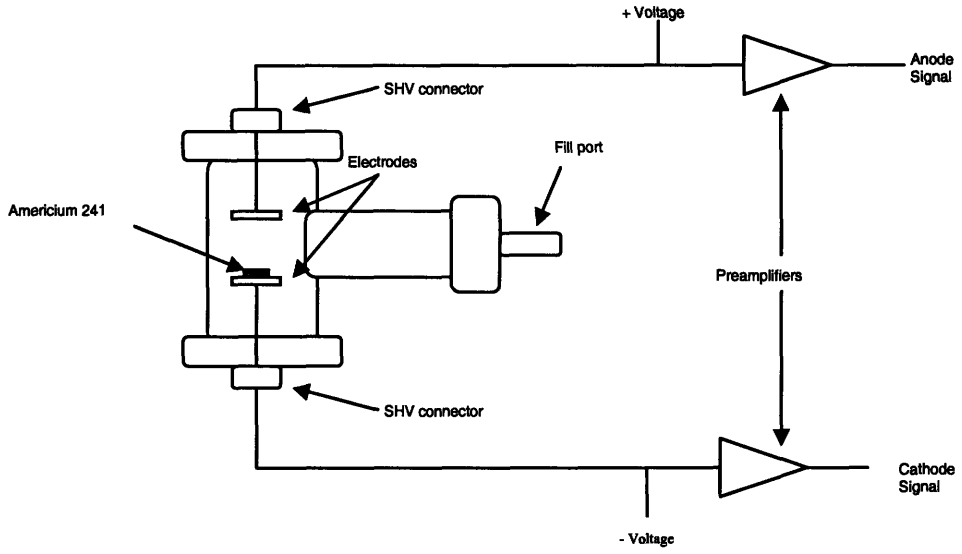

Figure 3.2 Illustration of the purity monitor design

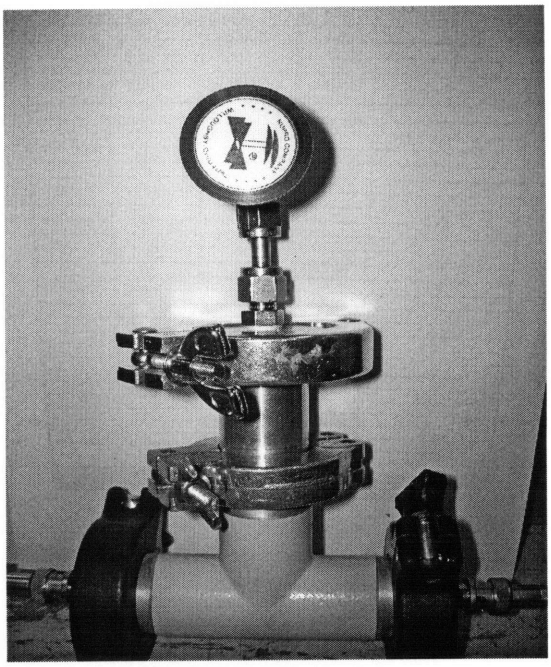

Figure 3.3 Photograph of purity monitor

Americium-241 is a man-made radioactive metal which decays primarily by alpha emission (5.5 MeV alphas) to neptunium-237. Low energy gamma radiation also accompanies the decays, the most prominent of which is the 59.5 keV gamma emissions. The half life of Am-241 is 432.2 years. The alpha particles emitted from the americium have short range so the ionization occurs relatively close to the cathode. The electrons flow from the cathode to the anode due to the electric field between the electrodes. The voltage applied to the anode was between 2000V and 3000V and the voltage applied to the cathode was between 1000V and 2000V. The electron lifetime is determined by comparing the charge signal amplitude measured from the cathode to that measured from the anode. The signals are each read from a low noise preamplifier (Canberra, model 2006) with a decay time constant of 50 μs.

Like the other chambers and the purification system, the purity monitor was cleaned before it was filled with dielectric liquid. The cleaning process consisted of an ethanol bath and a combination of baking and pumping for 15 hours.

Figure 3.4 displays the cathode and anode signals generated from the purity monitor filled with Isooctane. The positive voltage applied was 2000V and the negative

voltage was -1000V. The drift time is approximately 5.2μs. The electron lifetime, calculated via equation 3.2, is about 7.5μs. Ideally, the electron lifetime should be much greater than the electron drift time in order to collect the total charge produced in the chamber. However, electron-trapping impurities make achieving such electron lifetimes a challenge. As previously stated, the dielectric liquids are commercially sold with purities of about 99.9%, which corresponds to electron lifetimes of a few microseconds (1μs ≈ 1 ppm of O_2). Thus, one cycle through the purification system yields an improved purity of roughly 3 to 5 microseconds for Isooctane.

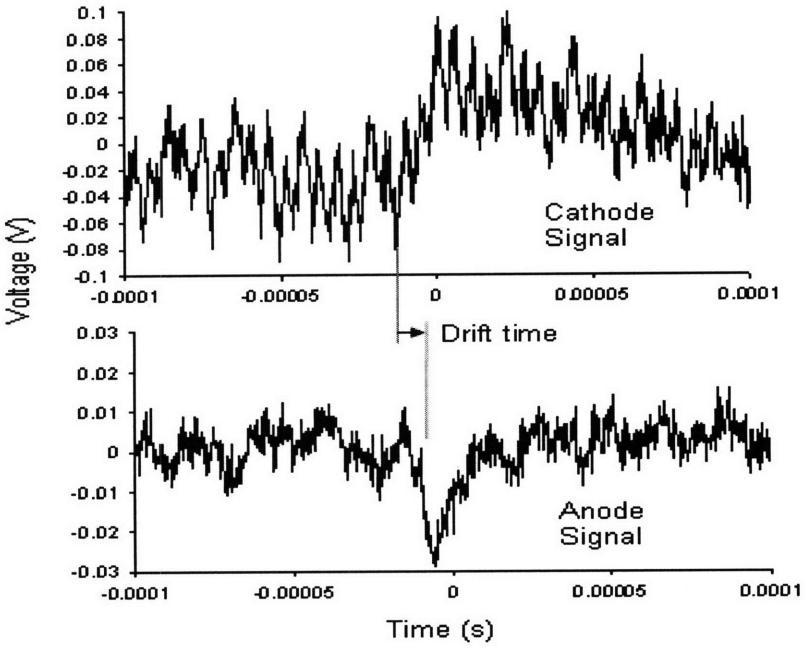

Figure 3.4 Measured cathode and anode signals from purity monitor filled with Isooctane

Figure 3.5 shows the cathode and anode signals generated from the purity monitor filled with TMS. The electron lifetime in TMS has been previously measured at values ranging between 5.5 to 450 microseconds at a 10kV/cm electric field between chamber electrodes [9], [20]. The electron lifetime of TMS measured from our purity monitor was approximately 175μs with drift time of about 144μs. The positive voltage applied was 2000V and the negative voltage was 1500V.

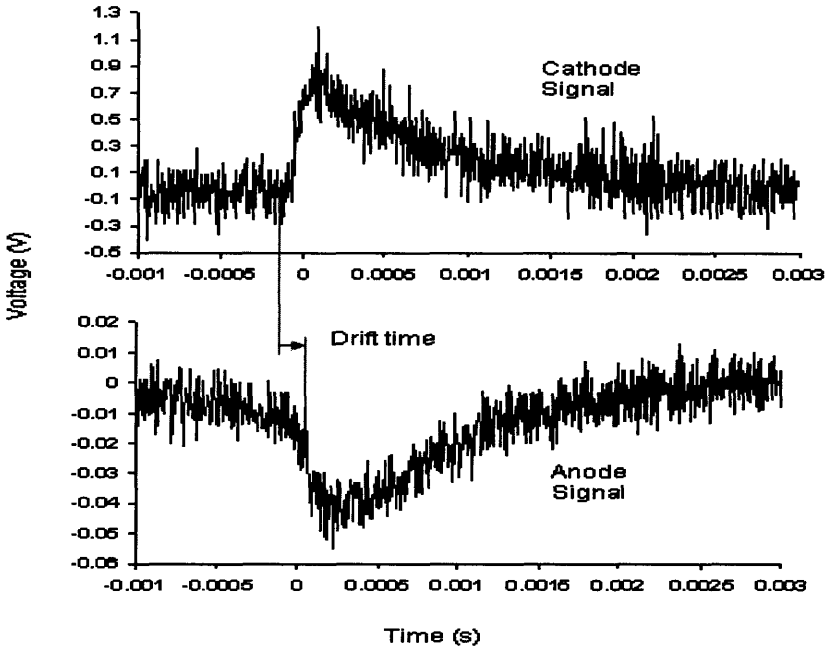

Figure 3.5 Measured cathode and anode signals from purity monitor filled with TMS

The electron lifetime of TMP has also been measured in other studies where the electron lifetimes achieved were between 30 and 50 microseconds at a 10kV/cm electric field [9], [20], [21]. Figure 3.6 shows the signal pulses obtained from our purity monitor when filled with TMP. The drift time was approximately 25μs and the electron lifetime was roughly 29.4μs. The voltage applied to the anode was 2000V and the voltage applied to the cathode was -1000V.

The achieved purity for TMP was not the result of one cycle through the purification system, as was the case with TMS and Isooctane. The TMP used in the experiment was donated to us by a group that was using the liquid for calorimeter experiments. Thus, the TMP had been previously purified. In addition, we purified the TMP at least 3 additional times when testing the functionality of the purification system. Only TMP was used to test the purification system because we had much more TMP available than the other two liquids.

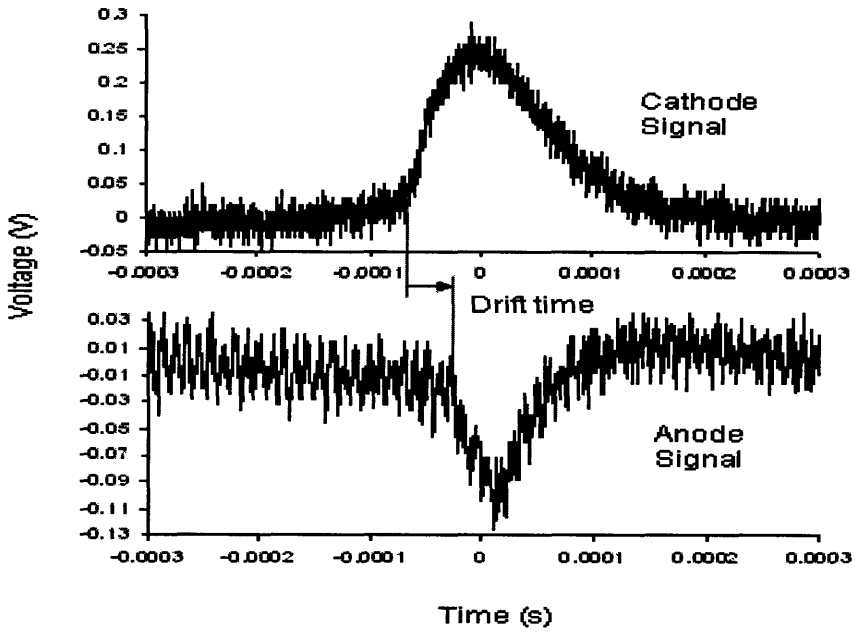

Figure 3.6 Measured cathode and anode signals from purity monitor filled with Isooctane

Electron Mobility and Drift Velocity

As stated above, the electron drift time is a function of the drift velocity at operating conditions. The drift velocity can be calculated using equation 3.7.

$$v = \mu E \qquad \text{Equation 3.7}$$

E is the electric field between the electrodes and μ is the electron mobility. The electron mobility for TMS, TMP, and Isooctane is 105±5 cm²/Vs, 29±2 cm²/Vs, and 7±2 cm²/Vs respectively [9], [24]. It is expected that as electron drift velocity increases, electron drift time would decrease. However, our results present the opposite effect. Based on the values for mobility given for each liquid, the drift time appears to decrease with decreasing drift time. This inconsistent behavior may be due to the impurities present in the liquids which can reduce mobility.

Discussion

A specific value for the purity required for the detecting fast neutrons is imprecise. The required purity is a function of the detector / purity monitor, the electric

field produced between the chamber electrodes and the liquid. Essentially, the liquid can be considered sufficiently pure when the purity monitor is capable of detecting single pulses of electrons. One study found that this happens at a purity of 10-50 ppb for TMS and TMP [10]. Another study shows that single electron pulses can be detected using TMS (commercially sold at 99.7%) and Isooctane (commercially sold at 99.5%) without additional purification.

We were successful at achieving signal pulses for all three liquids with the purity monitor; therefore, it appears one cycle through the purification system was satisfactory to achieve acceptable purities.

Chapter 4

Experimental Work

Chapter 4 concentrates on investigating whether the chambers we designed can be used as efficient detectors of fast neutrons. In the first experiments, we filled the chambers with P-10 gas and exposed them to x-rays produced at the 200kVp and 250 kVp settings. The current generated in the chamber was measured for various applied voltages. The purpose of this experiment was to confirm that the chambers were properly detecting radiation.

The second experiments entailed exposing the chambers filled with dielectric liquid to the x-rays. The current was measured at various applied voltages again. The objective of these experiments was to verify that the liquids were responding to radiation in the anticipated manner.

The final experiments comprised of exposing the dielectric liquid filled chambers to neutrons from a 1 Ci ^{239}Pu-Be source. The signals generated were counted and analyzed in order to investigate the sensitivity and efficiency of the detector.

4.1 X-ray Experiments

The x-ray experiments are considered a series of preliminary tests. The behavior of gas filled and dielectric liquid filled ionization chambers when exposed to photons has been previously studied [1], [10], [11]. A comparison of the behavior of our chambers to that of previously studied chambers (under similar operating conditions) allowed us to ascertain whether our chambers were operating properly. The analysis consisted of the observation of current-voltage characteristics. For each experiment, the current was measured from the high voltage supply (Bertan, 1792N).

In Chapter 2 it was stated that the dielectric liquids being studied are effectively gamma-blind due to low cross section values. It is shown in figures 2.1 through 2.3 that

the cross-section values are higher for low energy photons; thus, we expose the chambers to x-rays no more energetic than 250keV for these experiments. However, the energies must be large enough for the x-rays to successfully penetrate about an inch of stainless steel. We also exposed the chambers to 1μCi Co-60 (1173keV gamma) and Cs-137 (661keV gamma) check sources in order to test the gamma blindness of the chambers. No current increase or pulse signal could be measured with our electronics.

4.1.1 X-ray Source

The x-rays used for these experiments were generated from a Phillips RT250 Orthovoltage X-ray Unit, located in Building NW-14 room 1308. The RT250 x-ray machine is typically used for radiation therapy applications, but it was also sufficient for our purposes. It operates at fixed peak voltages of 75 kVp, 100 kVp, 150 kVp, 200 kVp, and 250 kVp. The beam current during operation was between 10 and 20 mA. The inherent filtration of the machine corresponds to 2mm aluminum. The additional filters available for the machine are listed in Table 4.1. In these experiments, the chambers were exposed to x-rays of each peak voltage. Consequently, the 0.4 Thoraeus filter was used because it is compatible with each peak voltage setting. The other filters have upper limits on the peak voltages they are compatible with.

Thoraeus is combination of 3 filters. The primary filter is tin, the secondary filter is copper, and the third filter is aluminum. The copper filter absorbs the characteristic radiation of the tin and the aluminum filter absorbs the characteristic radiation of the copper. The addition of the tin filter promotes hardening of the x-rays.

Table 4.1 Voltage and beam current settings with appropriate filters

Peak Voltage (kVp)	Beam Current (mA)	Filter
75	20	0.2mm Copper
100	20	0.35mm Copper
150	20	0.5mm Copper
200	17	1mm Copper
250	15	0.4 Thoraeus

(6mm lead filter also available)

4.1.2 Gas-Filled Ionization Chamber Experiments

Each of the chambers was filled with 30 PSI of P-10 gas before they were exposed to the x-rays. P-10 is a gaseous mixture of 90% argon and 10% methane. Argon is often used as a fill gas because it is a noble gas; thus, it does not react chemically with detector components. The addition of methane, a hydrocarbon gas, is exploited for quenching any excessive charge buildup.

Chamber 1

Chamber 1 was placed approximately 34 cm away from the x-ray tube. The chamber was oriented so that the photons would enter the chamber between the two electrodes. Figure 4.1 is an illustration of the setup.

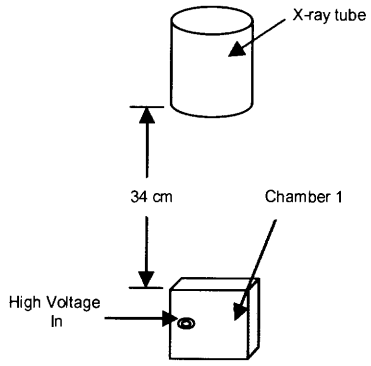

Figure 4.1 Illustration of setup for Chamber 1 x-ray experiment

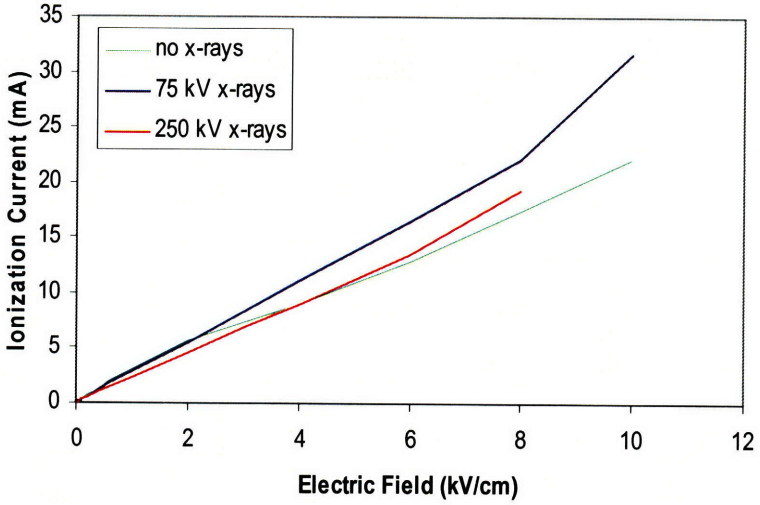

Figure 4.2 Ionization current against electric field strength for no x-rays, 75 kVp (I =13mA) x-rays, and 250 kVp (I = 10mA) x-rays in P-10 (chamber 1).

The measured relationship between current and voltage is approximately linear. The linear relationship indicates that the chamber is not working correctly. In theory, the current should saturate at a value much lower than 5000V (see Figure 4.3).

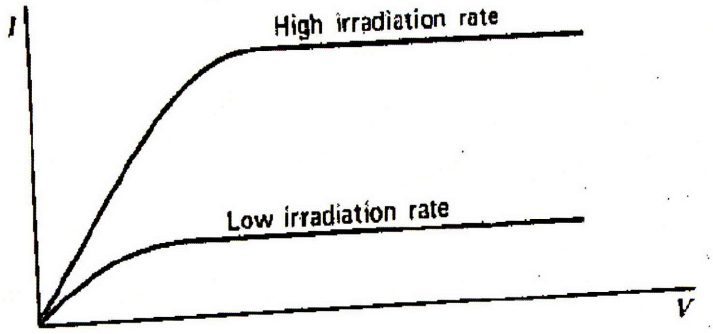

Figure 4.3 General current-voltage relationship of an ion chamber [1].

The current-voltage behavior exhibited in Figure 4.3 is initially linear. The linear region represents the recombination that occurs when the electric field is not high enough to maintain ion pair separation. As the voltage is increased, the electric field becomes strong enough to induce charge drift toward the respective electrodes. As a result,

recombination suppresses. At sufficiently large electric fields the recombination effects become diminutive and all the charges produced contribute to the measured current. The current value can no longer increase with voltage because all the charges have been collected and their rate of production is uniform [1].

Leakage current through the epoxy, between the electrodes, and through the rexolite are possible causes of the faulty detector behavior. Three observations are offered in support of this hypothesis. First, the resistance between the plates should be high enough that the current measurement is approximately zero when the chamber is not exposed to radiation. However, Figure 4.2 shows non-zero currents being generated without photon exposure. Secondly, the chamber is constructed of an insulator (rexolite). Insulators can readily accumulate surface deposits which represent pathways for leakage current. The epoxy used to seal the chamber is also insulating; thus, it could also serve as a leakage current pathway. Finally, a guard ring is not incorporated in the chamber design. The purpose of guard rings is to reduce electric field edge effects. The potential of the guard ring is held at roughly the same potential as the anode, which reduces charge leakage between the two electrodes.

Chamber 2

Chamber 2 was placed approximately 21 cm away from the x-ray tube. The chamber was oriented so that the photons would enter the chamber between the two electrodes. Figure 4.4 is an illustration of the setup.

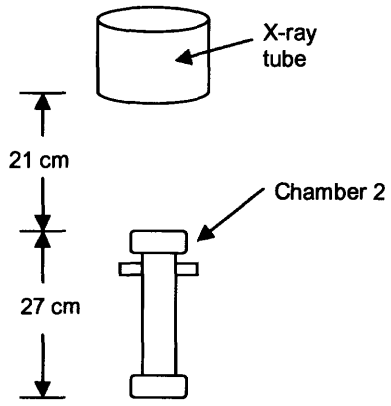

Figure 4.4 Illustration of setup for Chamber 2 x-ray experiment

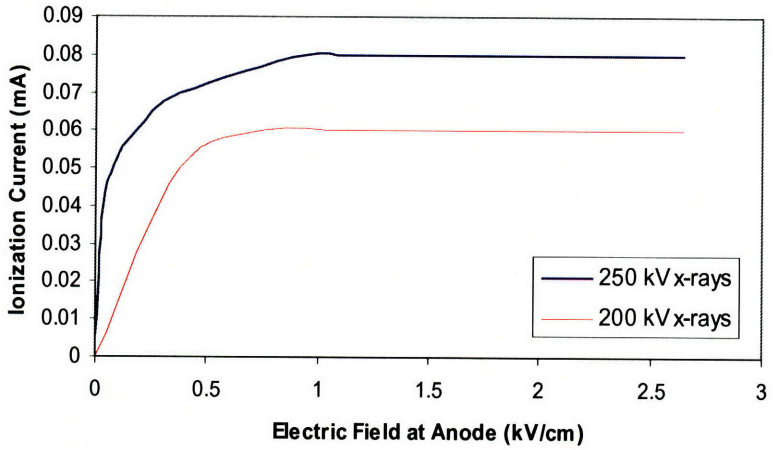

Figure 4.5 Saturation curve of 250 kV (I = 11mA) and 200 kV x-rays (I = 10mA) in P-10. (Chamber 2: Cylindrical chamber)

The current-voltage relationship shown in Figure 4.5 is consistent with expected detection behavior. Therefore, chamber 2 is considered to be working properly.

Chamber 3

Chamber 3 was placed about 40 cm away from the x-ray tube. The chamber could not be oriented to allow the photons to enter between the electrodes due to the chamber construction. The anode is separated from the bottom cathode with ceramic posts, but posts were not incorporated to separate the anode from the top cathode. Thus, if the chamber was oriented on its side or up-side down, the anode would be in direct contact with the cathode. Instead, the chamber was oriented such that the photons would enter the chamber though the ceiling of the chamber (top cathode). Figure 4.6 is an illustration of the setup.

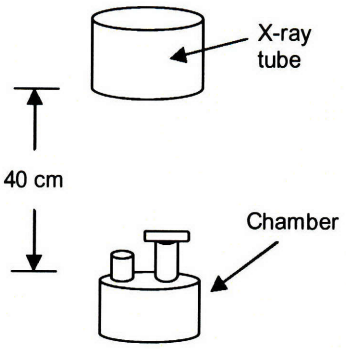

Figure 4.6 Illustration of setup for Chamber 3 x-ray experiment

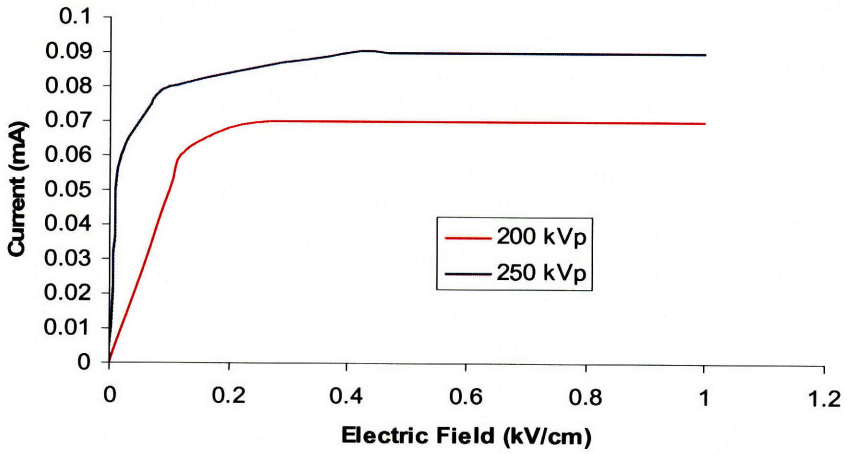

Figure 4.7 Saturation curve of 250 kV (I = 11mA) and 200 kV x-rays (I = 10mA) in P-10 (Chamber 3: Planar geometry).

The current-voltage relationship shown in Figure 4.7 is consistent with expected detection behavior. Thus, chamber 3 is also considered to be working properly.

4.1.3 Summary of Gas-Filled Ion Chamber X-ray Experiments

The results obtained in these experiments support the conclusion that chamber 2 and 3 are capable of detecting radiation and chamber 1, as is, is not. In addition to the deficient operation, chamber 1 also frequently acquired leaks. Due to the poor

performance and inferior construction of chamber 1, it was excluded from further detection experiments.

4.1.4 Dielectric Liquid Filled Ionization Chamber X-Ray Experiments

Chambers 2 and 3 were each filled with purified TMS, TMP, and Isooctane then exposed to x-rays produced at the 200kVp and 250kVp settings. The chambers were also exposed to the lower energy x-rays produced by the x-ray tube, but a current could not be measured. Various voltages were applied across the chamber electrodes and the current was monitored from the high voltage supply using a digital multimeter.

As previously discussed, the behavior of dielectric liquid ionization chambers exposed to gamma radiation has been previously studied. In these studies it has been determined that the ionization current will never saturate with respect to initial recombination. The ionization current will increase linearly with electric field when the liquid is under constant irradiation conditions and the electric field is high enough to suppress recombination.

Chamber 2

In these experiments, the chamber position in the x-ray unit was the same as it was in the gas filled ion chamber experiments. The behavior exhibited by the chamber when filled with each dielectric liquid, as seen in figures 4.8, 4.9, and 4.10, is consistent with the behavior observed in previous studies [10], [11].

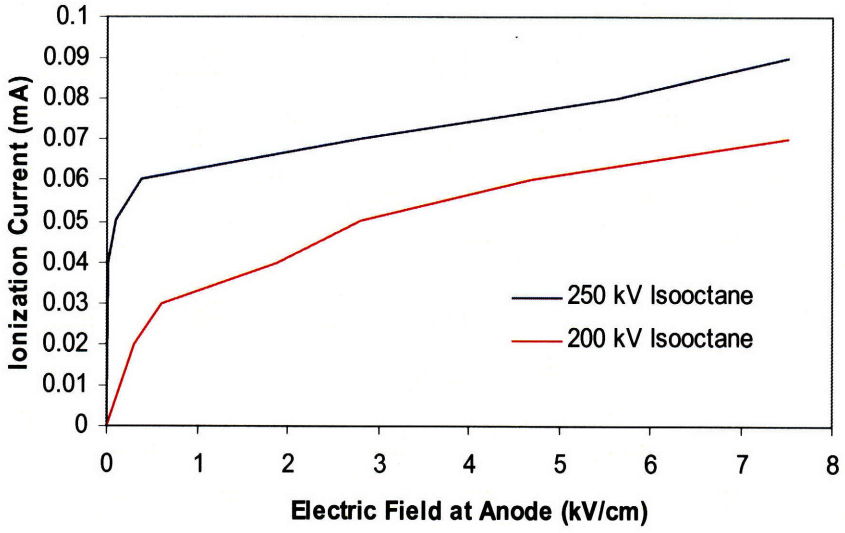

Figure 4.8 Ionization curve of 250 kV (I = 11mA) and 200 kV x-rays (I = 10mA) in Isooctane. (Chamber 2: Cylindrical chamber)

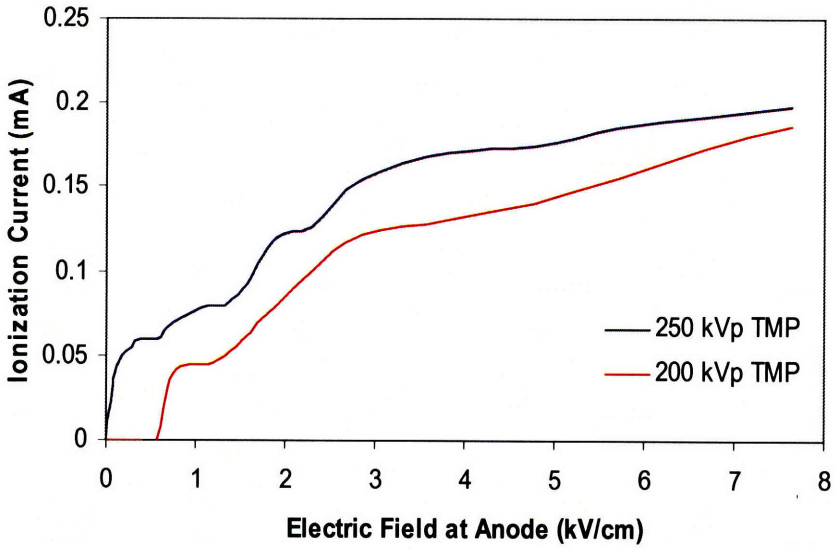

Figure 4.9 Ionization curve of 250 kV (I = 11mA) and 200 kV x-rays (I = 10mA) in TMP. (Chamber 2: Cylindrical chamber)

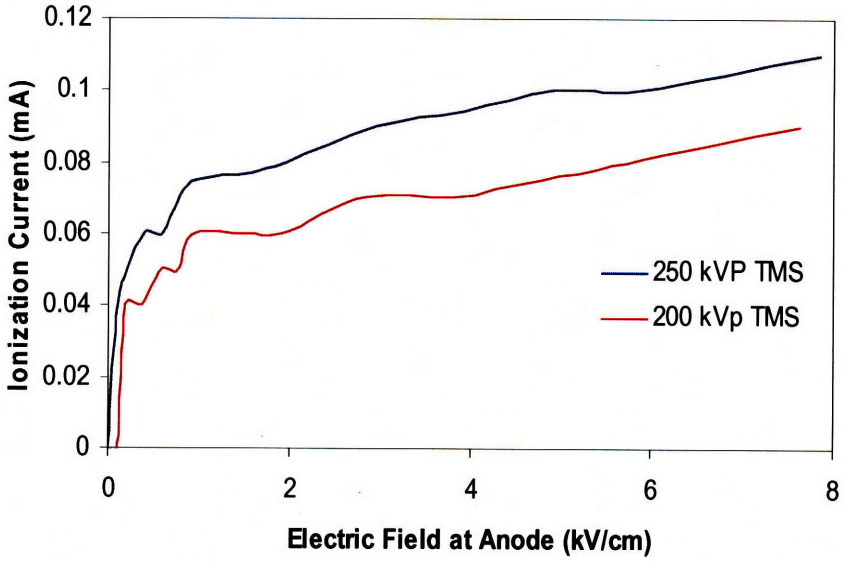

Figure 4.10 Ionization curve of 250 kV (I = 11mA) and 200 kV x-rays (I = 10mA) in TMS. (Chamber 2: Cylindrical chamber)

Chamber 3

Like chamber 2, the position of chamber 3 in the x-ray machine was the same as it was in the gas-filled ion chamber experiments. The relationship between current and electric field is shown in figures 4.11, 4.12, and 4.13.

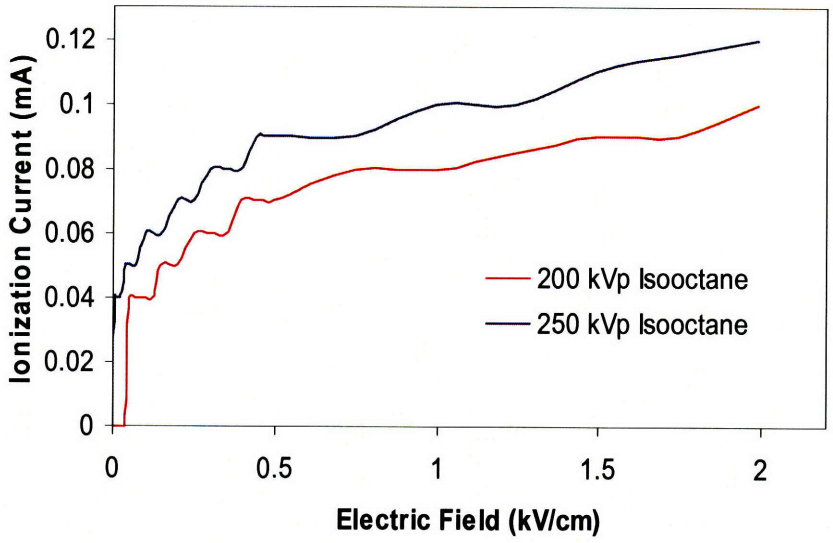

Figure 4.11 Ionization curve of 250 kV (I = 11mA) and 200 kV x-rays (I = 10mA) in Isooctane. (Chamber 3)

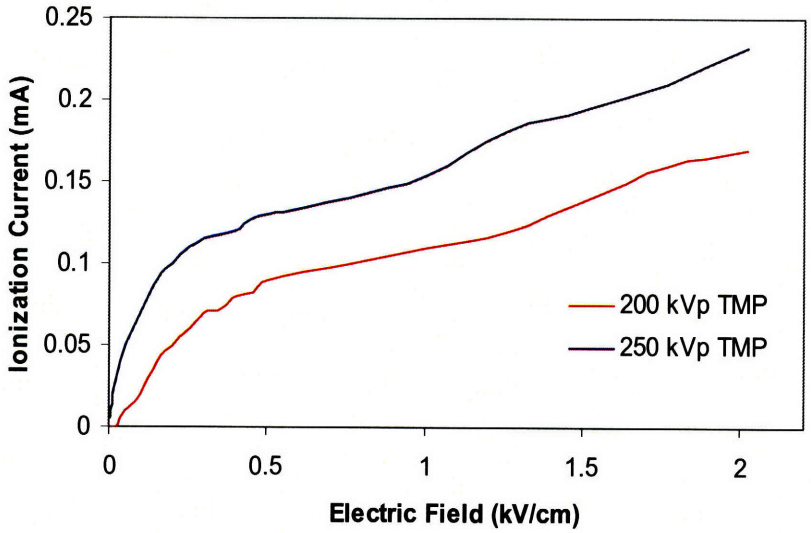

Figure 4.12 Ionization curve of 250 kV (I = 11mA) and 200 kV x-rays (I = 10mA) in TMP. (Chamber 3)

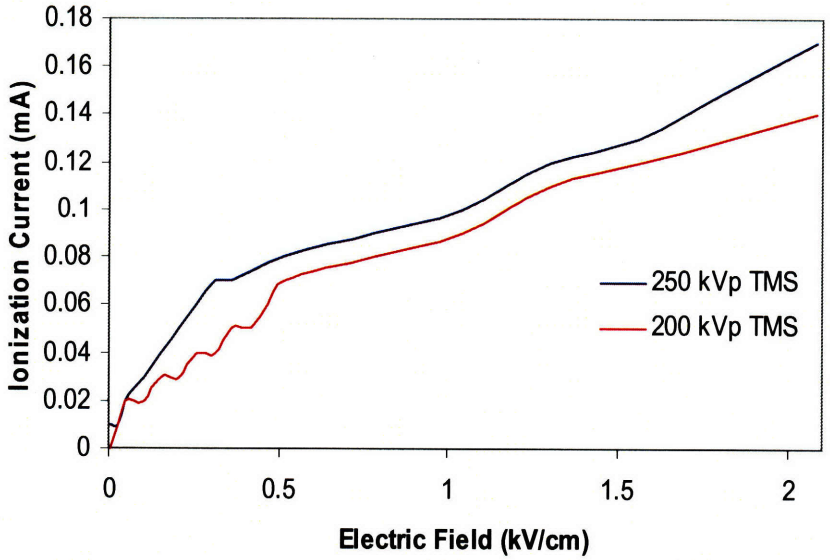

Figure 4.13 Ionization curve of 250 kV (I = 11mA) and 200 kV x-rays (I = 10mA) in TMS. (Chamber 3)

Figures 4.14 and 4.15 compare the ionization curves (250 kVp) for Isooctane, TMP, and TMS. TMP is found to yield higher ionization currents than TMS and Isooctane.

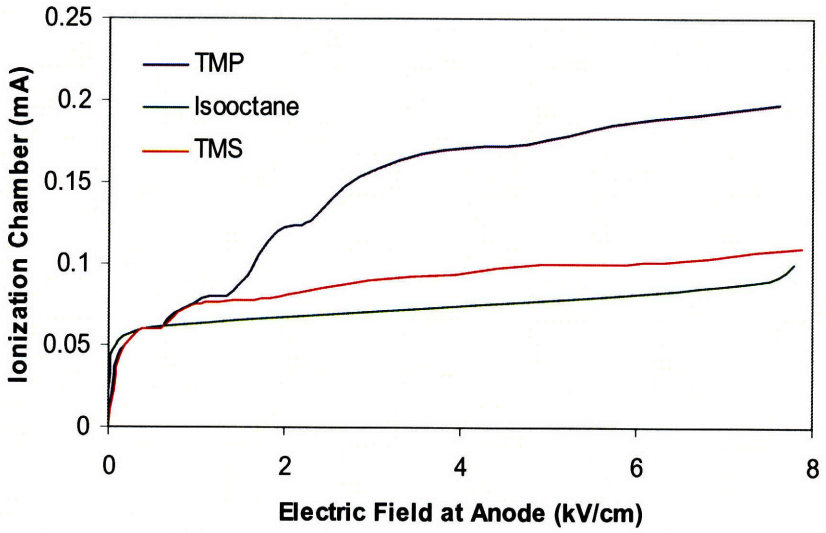

Figure 4.14 Ionization current for indicated liquids at various electric fields and 250kVp x-ray machine setting. (Chamber 2: Cylindrical Geometry)

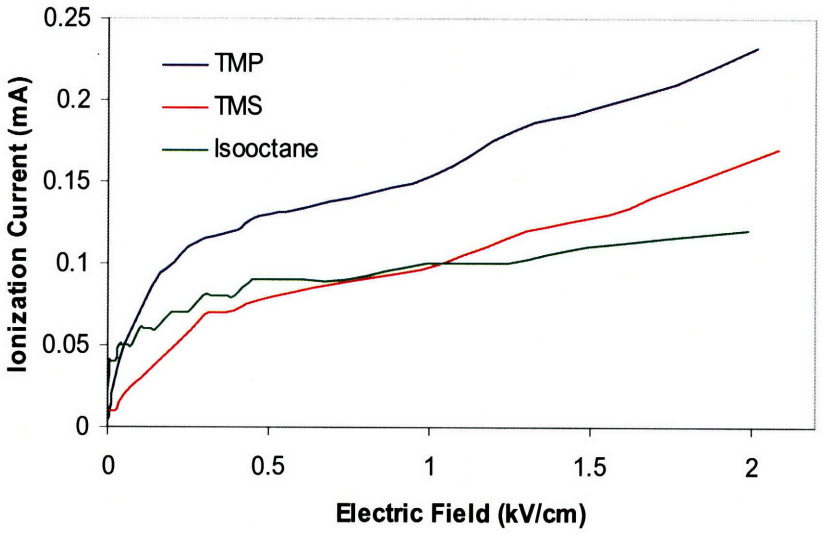

Figure 4.15 Ionization current for indicated liquids at various electric fields and 250kVp x-ray machine setting. (Chamber 3)

4.1.5 Summary of Dielectric Liquid X-Ray Experiments

The results obtained in these experiments confirm the results obtained in previous studies [10], [11]. We found that the ionization current at various electric fields, in fact does not saturate for the dielectric liquids we studied. In addition, the ionization current yield is much higher for TMP than the other liquids. This feature is a function of the higher G^{tot} value and purity of the TMP. G^{tot} is the total number of electrons released per 100eV deposited energy. The G^{tot} values for each of the liquids are listed in Appendix A. Contrary to our measurements, the ionization current yielded from TMS was expected to be similar to that of TMP because the G^{tot} values are similar for the two liquids and the purity measurement for TMS was adequate. On the other hand, our measurements are consistent with our expectation that Isooctane would yield a much lower ionization current than TMP because its G^{tot} value is about half that of TMP.

4.2 Fast Neutron Experiments

The chambers were exposed to fast neutrons emitted from a ^{239}Pu-Be source following the x-ray exposure experiments. These experiments are considered the crux of this thesis research because they answer our central question – whether or not ionization chambers filled with TMP, TMS, or Isooctane are capable of detecting fast neutrons. It was shown during purity monitoring, discussed in Chapter 3, that single pulses of electrons can be detected with dielectric liquid media. Nevertheless, the probability of a neutron interacting in the small active volume of the chambers is much smaller than that the alpha particles emitted from the americium. Thus, it is possible for a neutron to pass through the chambers without creating any electrons. In the x-ray experiments, it was shown that the chambers can detect uncharged particles; however, single pulses could not be measured in these experiments. The fast neutron detector is intended to be operated in pulse mode; therefore, the detection of single pulses is essential for successful functionality.

4.2.1 Neutron Source

The neutron source used in these experiments was a 1-Ci (3.7x 10^{10} Bq) ^{239}Pu-Be source. The neutron flux from the source is 1 x 10^{6} n/s and the mass of the ^{239}Pu is 15.99g. Additional characteristics of the source are listed in table 4.2.

Table 4.2 List of ^{239}Pu-Be source properties

Source	^{239}Pu-Be
Half-life	24000 y
E_α (MeV)	5.14
Neutron yield per 10^6 primary alpha particle	57
Percent yield with $E_n < 1.5$ MeV	9-33
Average neutron energy (MeV)	4.5
Peak neutron energy (MeV)	2.8

The ^{239}Pu-Be source is made by combining powdered Pu-239 with powdered Be-9. The powder mixture is encapsulated in stainless steel. Figure 4.16 is an illustration of the typical construction of a Pu-Be source.

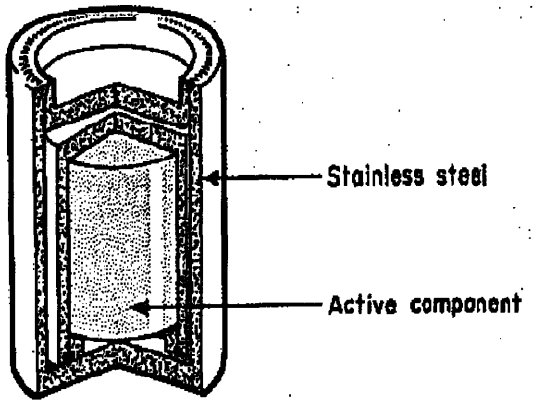

Figure 4.16 Double-walled construction of a Pu-Be source [1].

Pu-Be sources are isotropic and the neutrons are produced through the following exothermic nuclear reaction:

$$^{4}_{2}He+^{9}_{4}Be\rightarrow^{1}_{0}n+^{12}_{6}C+5.71MeV$$

The source emits neutrons and photons. The ^{239}Pu decay produces some low-energy x-rays, less than 20 keV, with a combined yield of about 4 percent. These x-rays are, for the most part, attenuated in the typical double stainless steel encapsulation. There is also a variety of low-yield, higher-energy gamma rays emitted in the decay process, with a combined yield of roughly 0.05 percent.

The energetic spectrum of neutrons is continuous with local maxima of 3 and 7-8MeV depending on the excitation state the ^{12}C product is left in [1]. The neutron spectrum ranges between 1.4 to 12MeV. Figure 4.17 is a neutron spectrum from a 1-Ci ^{239}Pu-Be source (common Pu-Be density of 5 g/cm^3) produced by Los Alamos National Laboratory (Sources-3A code) [23].

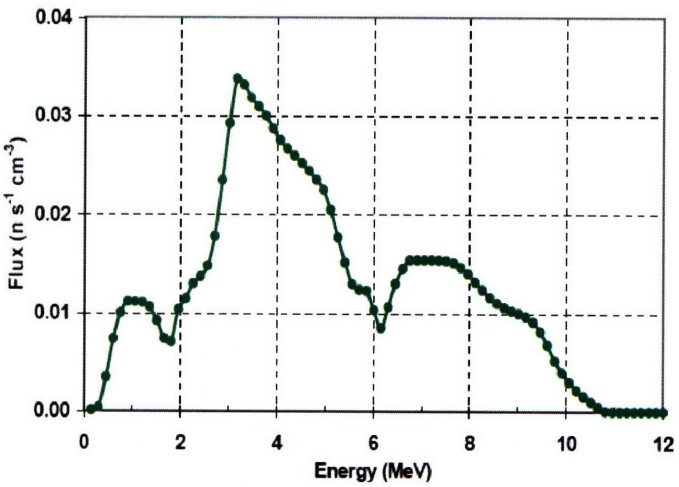

Figure 4.17 Calculated energy spectrum of neutrons from a 1-Ci ^{239}PuBe source [23].

4.2.2 Experimental Setup

Due to the strength of the neutron source we used for these experiments, the experiments were performed in the middle laboratory in the restricted area located in building NW-12. The experimental setup was the same for both chambers. The chambers were completely shielded with lead to attenuate any unwanted low energy gammas and the neutron source was placed on top of the lead. The neutrons from the source are energetic enough to traverse the lead without being attenuated. The source sits approximately 2 inches from the outside walls of the chambers. The electronics used to observe detector response are located about 4-5 feet from the chamber.

Chamber 2

The neutron experiments performed for chamber 2 consisted of filling the chamber with the liquids and counting the number of pulses observed in a 30 minute window. This process was done for various applied voltages. First, a 30 minute background count was taken and then the chamber was exposed to the source and another 30 minute count was performed. The counts were taken at the same applied voltage. The difference between the two count values represents neutrons that were detected at that applied voltage. The source was then taken away and another count was performed. It

was expected that the counts obtained should be similar to the background count subsequently taken.

The maximum voltage we applied to the anode of the chamber was 3000V. The voltage applied was limited by the preamplifier voltage threshold. The preamplifier specifications indicate that the high voltage through the preamp should not exceed 2000V. However, this is a conservative estimate because the capacitors in the preamplifier circuitry are 5000V capacitors. We did not attempt to run at 5000V in order to avoid blowing the preamplifier. The minimum applied voltage used for recording pulses was 2000V because the pulses usually became measurable at this voltage.

When voltage is first applied to the anode, the signals observed on the oscilloscope are chaotic. We suspect that the chaotic behavior was due to discharges within the liquid. The chamber was allowed to sit for a few hours with 3000V applied and afterward the signal stabilized. The applied voltage helps to further clean the dielectric liquids.

Chamber 2 Results

Chamber 2 successfully detected single pulses of electrons, but did not appear to respond to the neutron source. The background counts and the source exposure counts at various applied voltages for each liquid are given in table 4.3, table 4.4, and table 4.5. Although the source exposure counts are slightly higher than the background counts for Isooctane and TMS, the number of pulses that occur is a statistical process and the difference between the two count values is within the statistical error. Conversely, the behavior observed when Chamber 2 was filled with TMP was odd because the counts obtained for the source exposure were consistently much lower than the background counts. Currently, we are unsure why this behavior occurs.

A possible reason why the detector does not appear to detect neutrons is the low electric field at the cathode, which would allow the electrons produced from ionization to recombine before they reach the anode. When the voltage applied to the anode is 3000V, the corresponding electric field at the cathode is about .7kV/cm. The electric field at the anode would be about 5.6kV/cm. If the ionization occurs close to the anode, we would still expect to see a pulse because the electric field near the anode should be high enough

to suppress recombination. However, if the ionizations occur near the cathode, detection is unlikely because .7kV/cm is not a high enough electric field to suppress recombination (see figures 4.8-4.10). An interesting observation made during these experiments with Chamber 2 was that the pulse heights for most of the pulses were relatively equivalent. This could mean that the ionizations were occurring at the same distance from the anode and/or the same amount of energy was being deposited.

Table 4.3 Counts obtained for Chamber 2 filled with Isooctane at various applied voltages

Applied Voltage (V)	Background Count 1	Pu-Be Source Exposure Count	Background Count 2
2000	4	5	3
2500	27	29	25
3000	62	66	64

Table 4.4 Counts obtained for Chamber 2 filled with TMS at various applied voltages

Applied Voltage (V)	Background Count 1	Pu-Be Source Exposure Count	Background Count 2
2000	0	0	0
2500	0	0	0
3000	1	2	0

Table 4.5 Counts obtained for Chamber 2 filled with TMP at various applied voltages

Applied Voltage (V)	Background Count 1	Pu-Be Source Exposure Count	Background Count 2
2000	644	311	545
2500	842	377	727
3000	4101	735	4267

Chamber 3

The same method used to evaluate the detection performance of chamber 2 was used for chamber 3. However, due to the uniform electric field (inherent to parallel plate geometries), the field at the cathode of chamber 3 was higher than the field at the cathode of chamber 2 for the same applied voltage. Therefore, chamber 3 was expected to suppress recombination better than chamber 2. The maximum voltage applied to chamber 3 was 3000V and the minimum was 500V. Pulses began at a lower applied voltage for chamber 3 than for chamber 2, which was an effect of the electric field / chamber geometry.

Chamber 3 Results

Chamber 3 successfully detected single pulses of electrons and it also responded to the Pu-Be source when filled with TMP and Isooctane. The count rates significantly increased when the source was present and decreased back to background once the source was removed. Conversely, when chamber 3 was filled with TMS, it did not detect any background radiation nor did it respond to the Pu-Be source.

The background and source exposure counts at various voltages were recorded 3 times for TMP and Isooctane. The number of neutrons detected was the difference between the background counts and source exposure counts. The count differences obtained for each observation were averaged and plotted against applied voltage in figure 4.18 for Isooctane and 4.19 for TMP. The count values for each observation are listed in Appendix F.

The observed relationship between counts and applied voltage appears to be approximately linear for Isooctane and exponential for TMP. However, the small count range for Isooctane and statistical error could account for the observed difference in behavior. Error calculations for these experiments would be valuable future work.

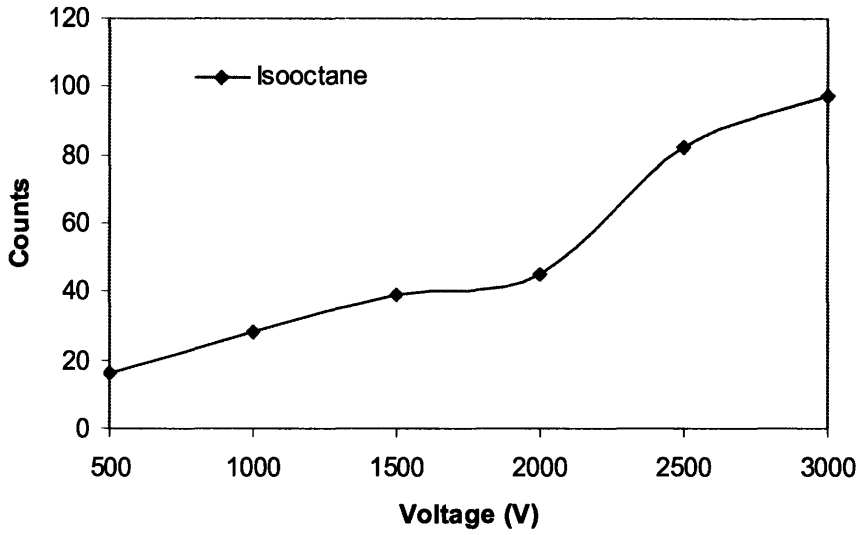

Figure 4.18 Plot of averaged neutron counts against applied voltage (Isooctane)

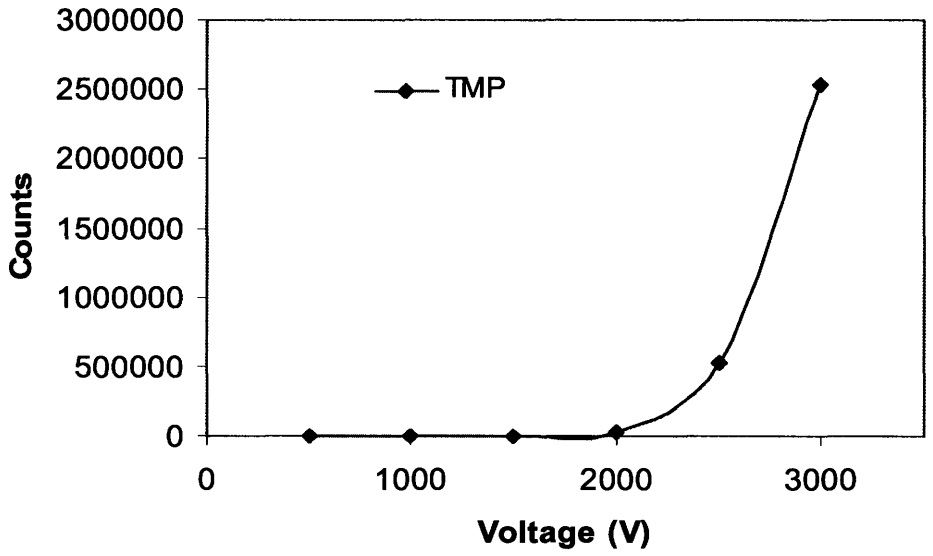

Figure 4.19 Plot of averaged neutron counts against applied voltage (TMP)

In Appendix E, the calculated absolute efficiency of TMS was lower than that of TMP and Isooctane for chamber 3. Thus, it is not surprising that when the chamber was filled with TMS it did not detect neutrons, but did when it was filled with TMP and Isooctane. The experimental absolute and intrinsic detection efficiencies for chamber 3

when filled with TMP and Isooctane were calculated using equation 2.7 and 2.3 respectively. The The Pu-Be source isotropicly emits approximately $1x10^6$ neutrons per second. Since the chamber is only exposed to one side of the source, we estimate the total number of neutrons exposed to the chamber to be $.5x10^6$ each second. The absolute and intrinsic efficiencies are given in Table 4.6 and Table 4.7 for chamber 3 filled with each liquid. The data in tables 4.6 and 4.7 support the conclusion that detection efficiency increases with applied voltage.

Table 4.6 Experimental Absolute and Intrinsic Efficiency values for Chamber 3 filled with Isooctane (30 minute observations)

Applied Voltage (V)	Absolute Efficiency (%)	Intrinsic Efficiency (%)
500	8.9E-7	1.8E-6
1000	1.6E-6	3.1E-6
1500	2.2E-6	4.3E-6
2000	2.5E-6	5.0E-6
2500	4.6E-6	9.1E-6
3000	5.4E-6	1.1E-5

Table 4.7 Experimental Absolute and Intrinsic Efficiency values for Chamber 3 filled with TMP (30 minute observations)

Applied Voltage (V)	Absolute Efficiency (%)	Intrinsic Efficiency (%)
500	3.9E-7	7.8E-7
1000	2.3E-4	4.7E-4
1500	2.4E-4	4.8E-4
2000	1.4E-3	3E-3
2500	.03	.06
3000	.14	.28

4.2.3 Summary of Neutron Exposure Experiments

The results of these experiments support the conclusion that chamber 3, filled with TMP or Isooctane, is capable of detecting fast neutrons from a ^{239}Pu-Be source, although the efficiency is extremely low. Chamber 2 (for all three liquids) and chamber 3 (filled with TMS) failed to respond when exposed to the source. Possible explanations and improvements are presented in Chapter 5.

Chapter 5

Conclusions

The results of this work indicate that dielectric liquids, namely TMP and Isooctane are promising media for fast neutron detectors. Although it was not completely demonstrated in this thesis that an ionization chamber filled with TMS is capable of detecting fast neutrons, the prospect still exists for success if the purity of TMS is improved further and higher electric fields are achieved. Additional successes and failings of this research are discussed in more detail in the following sections of this chapter. The shortcomings experienced in this work were mostly due to chamber design, liquid impurities, and applied voltage limitations. The main disappointment of this work was the low detection efficiencies obtained. Suggestions for how to improve efficiency are offered later in this chapter.

5.1 Project Successes

The main goal of this work was to design and construct dielectric liquid ionization chambers that effectively detect fast neutrons. This goal was met with Chamber 3 when filled with Isooctane or TMP; however, the detector is more efficient when filled with TMP. To achieve the central goal, other successes were attained along the way. For instance, our method used to monitor purity was successful. In addition, we conclude that the purification system and process was effective because the purity of the commercial grade liquids improved after one cycle through the system. The results from the x-ray experiments we performed and the electron lifetime (purity) values we measured were consistent with published results from other studies.

5.2 Project Shortcomings

While the successes achieved in this work are respectable, there are many improvements that can be incorporated to address shortcomings and improve overall results. A major limiting factor in this research was the high voltage constraint. In most of the references we used, the chambers were operated at electric fields of approximately 10kV/cm [9], [11], [25]. At 3000V, our maximum voltage, the electric field in chamber 3 was about 3 kV/cm and 6kV/cm (.7kV/cm) at the anode (cathode) of chamber 2 (dielectric constant of ~2). It was previously concluded that efficiency improves with increased voltage; thus, herein lies a likely explanation for the low efficiencies we acquired with our chambers.

Chamber 1

The fundamental problem with chamber 1 was the design. Constructing the chamber out of *Rexolite* was attractive because of its insulating properties and moderate transparency. The transparency of the chamber makes it easy see when the chamber is filled with the liquid, which was discussed in detail in chapter 3. Constructing the chamber with an insulating material, such as *Rexolite*, is also beneficial because the chamber could be used as a purity monitor. Thus, incorporating purity monitoring into the purification system becomes an option.

A disadvantage of using *Rexoite* for the detector casing is its sensitivity to noise. Chambers 2 and 3 were made out of stainless steel so shielding was incorporated in their design, but chamber 1 needed external shielding. In order to shield chamber 1, it was encased in a steel box which did help to reduce noise, but not enough to allow for a readable signal. Without the steel box, the noise coming out of the detector and preamplifier combined was 200mV. After the addition of the box, the noise was reduced to 30mV. The addition of an amplifier would only amplify the noise out of the preamplifier. For comparison, the noise output was essentially just that of the preamplifier and amplifier for chamber 2 and 3 - approximately 1mV out of the preamp and 300mV out of amplifier (gain 200) for chamber 2 and 4mV out of the preamp and 1000V out of the amplifier (gain 200) for chamber 3.

The *Rexolite*, was not the only design complication of chamber 1. The use of epoxy to seal the chamber was also a major issue. The epoxy we used did not efficiently keep the chamber sealed under pressure and it appeared to be somewhat conductive, although it was a dielectric epoxy. The design of chamber 1 would have been more robust if a better way to seal the chamber was exploited, such as o-rings.

Chamber 2

The central problem with chamber 2 is the geometry. Due to the combination of the non-uniform electric field in the chamber (inherent to a cylindrical geometry) and the voltage limitations, the detection of fast neutrons was not accomplished. Another issue with chamber 2, as previously discussed, is the fact that determining when the chamber is filled is difficult to do because of the stainless steel chamber walls, which however serve as effective shielding.

Chamber 3

Chamber 3 yielded the best results in this research. It was the only chamber that was successful at detecting neutrons, albeit, with very low efficiency. Again, it was difficult to determine when the chamber was full with liquid, but another port could be added to the top of the chamber such that when the liquid begins to exit the added port, the chamber is full. The uniform electric field produced due to the parallel plate construction is concluded to be essential for detecting fast neutrons when extremely high voltages cannot be applied.

5.3 Suggestions for Future Work

There are many modifications that can be made to improve the performance of the detectors and purification system, some of which are listed below.

- Redesign the chamber so that it can serve as the purity monitor
- Incorporate the purity monitor into the purification system so that the liquid can be continuously circulated through the system until it is sufficiently purified. The

modification eliminates the additional transfer of the liquid from a separate purity monitor to the detector.

- Redesign the chamber so that the electric feedthroughs can withstand higher applied voltages.
- Incorporate a preamplifier that can withstand at least 10 kV into the electronics setup or redesign the chamber so that the high voltage can be applied directly to the chamber instead of through the preamplifier.
- Construct arrays of chambers to achieve more sensitive volume; thus, higher efficiency.
- Incorporate "Frisch grids" into the chambers to obtain incoming radiation energy information.
- Expose detectors to a monoenergetic pulsed neutron source (i.e. accelerator, neutron generator) in order to obtain efficiency values for various neutron energies.

In addition to the ionization properties of the dielectric liquids, their scintillation properties would also be a study of interest. The scintillation properties of condensed noble gases have been previously studied and show good results; however, refrigeration systems for maintaining cryogenic temperatures are often an expensive necessity for their use. Detection methods that rely on the scintillation properties of noble liquids are often used for extremely large systems.

References

[1] Knoll,G., Radiation Detection and Measurement, John Wiley & Sons, Inc., 1989.

[2] Kobayashi, M., Introduction to Scintillators, http://nicadd.niu.edu/research/extruder/extruder_files/doc/Scintillator%20Radiation%20Damage/radiation.doc.

[3] Horvath. A., Ieki, K., et al, "Comparison of Two Liquid Scintillators used for Neutron Detection". *Nuclear Instruments and Methods in Physics Research A,* Vol. 440, No.1, 2000, pp 241-244.

[4] Hansen, R.R., Reeder, P.L., et al, "Neutron-Gamma Discrimination in Plastic Scintillators". *IEEE* 1999.

[5] EG&G Ortec, "Neutron-Gamma Discrimination with Stilbene and Liquid Scintillators", http://www.ortec-online.com/res_apps/res_timing.htm, 1989.

[6] Chen, G., "Fast Neutron Resonance Radiography for Elemental Imaging: Theory and Applications" Masters Thesis 2001.

[7] Table of Physical Constants of Scintillators, http://www.eljentechnology.com/datasheets/quicktable2002.pdf.

[8] Cylindrical chamber picture, http://hyperphysics.phyastr.gsu.edu/hbase/electric/imgele/ccyl.gif

[9] Engler J., "Liquid Ionization Chambers at Room Temperature", *Journal of Physics G: Nucl. Part. Phys.* Vol. 22, No.1, 1996, pp 1-23.

[10] Berghofer T., Eberle K., "Liquid Ionization Chambers for Radiation Therapy", 2005.

[11] Holyroyd, R., Anderson, D., "The Physics and Chemistry of Room-Temperature Liquid-Filled Ionization Chambers", *Nuclear Instruments and Methods in Physics Research A,* 236, 1985, pp. 294-299.

[12] Tanaka, H , Ariyoshi, T, et.al., "Study of the liquid-methane ionization chamber", *Nuclear Instruments and Methods in Physics Research A,* 539, 2005, pp. 613-621.

[13] Spherical chamber picture, http://hyperphysics.phyastr.gsu.edu/hbase/electric/imgele/csph.gif

[14] Marrone, S., Cano- Ott, D., et al., "Pulse shape analysis of liquid scintillators for neutron studies". *Nuclear Instruments & Methods in Physics Research A,* 490, 2002, pp 299-307.

[15] Denbow, J., "Recombination in Liquid Argon", University of Michigan REU at Nevis Laboratory, Columbia University, 2001.

[16] Stromswold, D.C., Peurrung, A.J., et al., "Direct Fast-Neutron Detection", Pacific Northwest National Laboratory.

[17] Jastaniah, S.D., Sellin, P.J., "Digital techniques for n/γ pulse shape discrimination and capture-gated neutron spectroscopy using liquid scintillators". Vol 517, Issues 1-3, 2004, pp 202-210.

[18] Cennini, P., Cittolin, S., et al., "Argon purification in the liquid phase". *Nuclear Instruments & Methods in Physics Research section A*, 33, 1993, pp 567-570.

[19] Badertscher, A., Laffranchi, M., Rubbia, A., "Development of a novel high-sensitvity LAr purity monitor based on an alpha source", *Elsevier Science*, 2006.

[20] Engler J., F. Fessler et al., "A warm-liquid calorimeter for cosmic-ray hadrons", *Nuclear Instruments and Methods in Physics Research A*, 427, 1999, pp 528-542.

[21] Poffenberger, P.R., Bishop, S., et al., "Operation of an ion chamber consisting of lead plates immersed in 2,2,4,4 - tetramethylpentane", *Nuclear Instruments and Methods in Physics Research Section A*, 426, 1999, pp 356-365.

[22] Johansson, B., Wickman, G., "General collection efficiency for liquid isooctane and tetramethylsilane used as sensitive media in a parallel-plate ionization chamber". *Phys. Med. Biol.* Vol. 42, 1997, 133-145.

[23] Craig-Alan C. Bias, Major. "Optimizing the Detection of Neutrons from Small-Quantity Weapons-Grade Nuclear Materials", Masters Thesis, Colorado State University, Department of Radiological Health Sciences, May 2002.

[24] Schmidt, W., Allen, A.O., "Mobility of Electron in Dielectric Liquids" *The Journal of Chemical Physics*, Vol. 52, No. 9, 1970.

[25] Neuman, D., Undergraduate Thesis, San Francisco State University, 1996.

Appendix A: Pulse Height Calculations

$$q_e = \frac{q}{2} = \frac{ne}{2} = \frac{E_n e}{4W}$$

where q is the total charge of ion pair and $E_n/2$ is the average fraction of energy transferred from the incoming neutron to the recoil proton.

Let $E_n = 4.5 \times 10^6$ eV, let d = 5mm, let x = 2.5 mm, and let $C = 1 \times 10^{-12}$ F

$e = 1.60 \times 10^{-19}$ C

TMS

$G_{tot} = 3.0$

$$V_{electrons} = \frac{E_n xeG_{tot}}{4Cd(100eV)} = \frac{(4.5x10^6 eV)(2.5x10^{-3} m)(1.60x10^{-19} C)(3.0)}{4(1x10^{-12} F)(5x10^{-3} m)(100eV)} = 2.70mV$$

TMP

$G_{tot} = 3.2$

$$V_{electrons} = \frac{E_n xeG_{tot}}{4Cd(100eV)} = \frac{(4.5x10^6 eV)(2.5x10^{-3} m)(1.60x10^{-19} C)(3.2)}{4(1x10^{-12} F)(5x10^{-3} m)(100eV)} = 2.88mV$$

Isooctane

$G_{tot} = 1.83$

$$V_{electrons} = \frac{E_n xeG_{tot}}{4Cd(100eV)} = \frac{(4.5x10^6 eV)(2.5x10^{-3} m)(1.60x10^{-19} C)(1.83)}{4(1x10^{-12} F)(5x10^{-3} m)(100eV)} = 1.65mV$$

Appendix B: Sensitive Volume Calculations

CHAMBER 1:

The dimensions of the both electrodes in chamber 1 are 3" x 3" (7.62cm x 7.62cm). The electrode separation is .5 cm.

$$V_{sensitive} = l \times w \times h$$

Therefore, the sensitive volume is $29cm^3$ [7.62cm x 7.62cm x .5cm].

CHAMBER 2:

The inner and outer electrodes of chamber 2 are cylindrical shells. The inner diameter of the outer electrode is .805" (2.0447cm) and the outer diameter of the inner electrode is .12" (.3048cm). The length of both electrodes is 8.5" (21.59cm).

$$V_{sensitive} = V_{cathode} - V_{anode} = \pi l(b^2 - a^2)$$

In the above equation, b is the inner radius of the cathode, a is the outer radius of the anode, and l is the length of the electrodes. Thus, the sensitive volume is $69.31cm^3$ [π x 21.59 x (1.02235^2 - $.1524^2$].

CHAMBER 3:

This chamber is designed to have two sensitive volumes. The first is the volume between the center electrode and the ceiling of the chamber and the second is the volume between the center electrode and basement of the chamber. The cathodes and anode are circular in shape so; although, the plate geometry of the chamber is planar, the sensitive volume is calculated using an equation for cylindrical geometry.

$$V_{sensitive} = 2\pi r^2 d$$

In the above equation, r is the radius of the anode (4.19cm), d is the distance between the anode and cathode (.5cm), and the factor of 2 is necessary because there are two equivalent sensitive volumes. The total sensitive volume for chamber 3 is $55.15cm^3$ [2 x π x $(4.19cm)^2$ x (.5cm)].

Appendix C: Electric Field Calculations

CHAMBER 1:

The plate geometry of chamber 1 is planar; thus, the equation used to calculate the electric field between the electrodes is

$$E = \frac{V}{\varepsilon_r d}$$

V is the voltage applied across the electrodes, d is the separation distance between the electrodes, and ε_r is the dielectric constant of the detection medium. The electric field desired for our applications is 10kV per cm. Thus, since the separation distance is .5cm and the dielectric constants for TMS, TMP, and Isooctane are 1.92, 1.98, and 2.01 respectively, the voltage applied between the plates must be 9600V for TMS, 9900 for TMP, and 10kV for Isooctane.

CHAMBER 2:

Due to the radial dependent (1/r) electric field produced by the electrode geometry of chamber 2, calculating the field throughout the chamber is more complex than for planar geometry. Typically, analytical methods are exploited to perform the calculation. However, the electric field at various points in the chamber can be calculated if the radius where the points are located is known. The equations below are used to calculate electric field at the anode (outer) surface and cathode (inner) surface.

$$E_a = \frac{V}{\varepsilon_r a \ln(b/a)} \qquad E_b = \frac{V}{\varepsilon_r b \ln(b/a)}$$

V is the voltage applied across the electrodes, a is the (outer) anode radius, and b is the (inner) cathode radius . To maintain an electric field of 1kV per mm (10kV/cm) at the anode, the voltage across the plates would need to be approximately 5568V for TMS,

5742V for TMP, and 5829V for Isooctane. With these voltages, the electric field at the cathode would be 776V/cm for TMS, 753V/cm for TMP, and 741V/cm for Isooctane. Maintaining an electric field of 10kV/cm at the cathode is unrealistic because the necessary voltage applied across the electrodes would have to be around 40,000V when the detection medium is one the three dielectric liquids discussed.

CHAMBER 3:

The electrode geometry of chamber 3 is planar so the electric field can be calculated using the same equation used for calculating the electric field in chamber 1. The plate separation is .5cm; therefore, to maintain an electric field of 10kV/cm, the voltage applied across the electrodes must be 9600V for TMS, 9900V for TMP, and 10kV for Isooctane.

Appendix D: Solid Angle Calculations

CHAMBER 1:

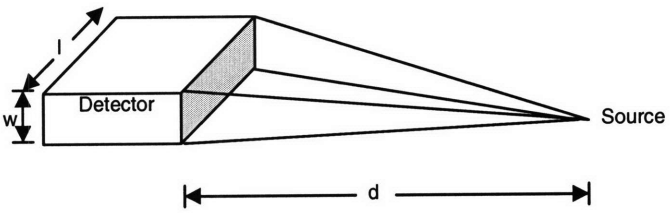

$$\Omega = \frac{l \times w}{d^2}$$

The surface area of the detector face directed toward the source is (l = 3cm; w = .5cm) 1.5 cm² and the distance between the detector and the source is d. At d equal to 10cm, the solid angle is .15 steradians.

CHAMBER 2:

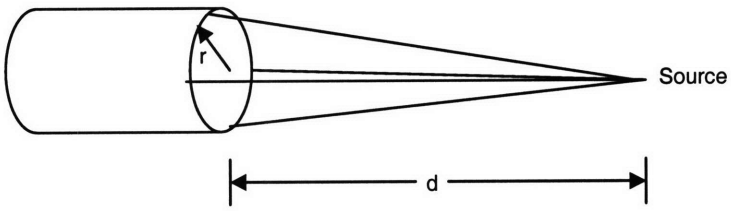

$$\Omega = \frac{\pi r^2}{d^2}$$

The surface area of the detector face directed toward the source is (r = .87cm) 2.38cm^2. At d = 10cm, the solid angle is .24 steradians.

CHAMBER 3:

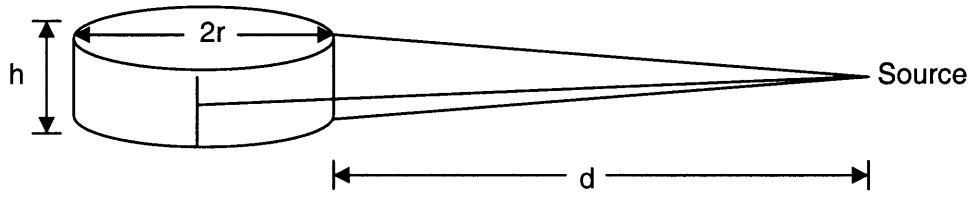

Calculating the solid angle for this chamber is more difficult than for the previous two chambers because the detector entire face directed toward the source is not equi-distanced from the source. A rough estimate of the solid angle is calculated by modifying the detector face such that it is flat and rectangular. This is done by placing the detector face a distance of d+.5r from the source. The modification is illustrated is below.

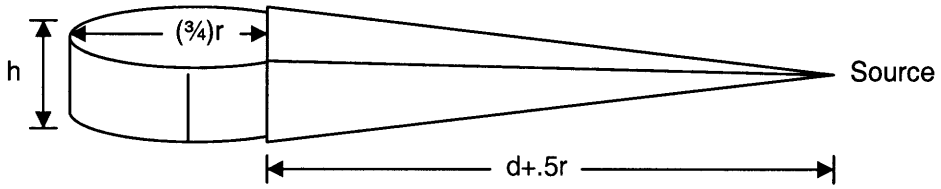

The surface area of the modified detector face is estimated at approximately 3.3cm x 1cm. 3.3cm is actually the electrode diameter and 1cm is the sum of the distance between the center electrode and the ceiling of the chamber and the distance between the center electrode and the basement of the chamber. Therefore, if the distance between the source and the modified detector face is (r = 1.65cm; d= 10cm) 10.825cm, the estimated value for solid angle is .31 steradians using the following equation.

$$\Omega = \frac{electrode.diameter \times h}{d + .5(electrode.radius)}$$

Appendix E: Calculated Efficiency Values

Table E.1 Calculated intrinsic efficiencies (%) for TMS, TMP, and Isooctane for each chamber

Energy (MeV)	Chamber 1			Chamber 2			Chamber 3		
	TMS	TMP	Isooctane	TMS	TMP	Isooctane	TMS	TMP	Isooctane
2	61.4	67.5	66.8	78.0	79.1	79.2	63.9	69.5	69.0
6	40.9	47.6	46.8	68.7	72.8	72.5	43.6	50.4	49.5
10	30.1	35.8	35.0	58.1	63.5	62.9	32.3	38.2	37.4
14	22.8	27.2	26.6	46.1	50.6	50.0	24.6	29.2	28.6
18	18.3	22.0	21.5	38.8	43.1	42.6	19.8	23.7	23.2

Table E.2 Calculated absolute efficiencies (%) for TMS, TMP, and Isooctane for each chamber

Energy (MeV)	Chamber 1			Chamber 2			Chamber 3		
	TMS	TMP	Isooctane	TMS	TMP	Isooctane	TMS	TMP	Isooctane
2	.733	.805	.798	1.49	1.51	1.51	1.55	1.69	1.67
6	.488	.569	.558	1.31	1.39	1.38	1.06	1.22	1.20
10	.359	.427	.418	1.11	1.21	1.20	.78	.92	.91
14	.272	.325	.317	.88	.97	.96	.57	.70	.69
18	.219	.263	.257	.74	.82	.81	.48	.58	.56

Appendix F: Counts Obtained in Pu-Be Exposure Experiments

Table F.1 Observation 1: Chamber 3 filled with Isooctane

Voltage (V)	Background Count #1	Source Exposure Count	Background Count #2	Detected Neutron Count (range
500	0	16	0	16
1000	0	28	0	28
1500	0	39	1	39
2000	0	45	2	43-45
2500	82	116	85	31-34
3000	41	56	38	15-18

Table F.2 Observation 2: Chamber 3 filled with Isooctane

Voltage (V)	Background Count #1	Source Exposure Count	Background Count #2	Detected Neutron Count
500	-	-	-	-
1000	-	-	-	-
1500	-	-	-	-
2000	0	52	1	51-52
2500	8	139	1	131-138
3000	53	145	66	79-92

Table F.3 Observation 3: Chamber 3 filled with Isooctane

Voltage (V)	Background Count #1	Source Exposure Count	Background Count #2	Detected Neutron Count
500	-	-	-	-
1000	-	-	-	-
1500	-	-	-	-
2000	-	-	-	-
2500	1	139	0	138-139
3000	10	111	-	101

Table F.4 Observation 1: Chamber 3 filled with TMP

Voltage (V)	Background Count #1	Source Exposure Count	Background Count #2	Detected Neutron Count (range)
500	0	11	3	8-11
1000	0	1981	6	1975-1981
1500	16	3928	32	3896-3912
2000	438	21410	601	20809-20972
2500	10413	554832	13098	541734-544419
3000	59981	4263950	72571	4191379-4203969

Table F.5 Observation 2: Chamber 3 filled with TMP

Voltage (V)	Background Count #1	Source Exposure Count	Background Count #2	Detected Neutron Count
500	0	2	-	2
1000	0	7318	-	7318
1500	7	7781	-	7774
2000	213	25699	-	25486
2500	12652	413925	-	401273
3000	53966	1053374	-	999408

Table F.6 Observation 3: Chamber 3 filled with TMP

Voltage (V)	Background Count #1	Source Exposure Count	Background Count #2	Detected Neutron Count
500	0	9	-	9
1000	0	3351	-	3351
1500	3	1346	-	1343
2000	559	33772	-	33213
2500	11627	662355	-	650728
3000	62569	2481033	-	2418464